

# Modeling gravitational radiation from coalescing binary black holes

J. Baker,<sup>1</sup> M. Campanelli,<sup>2,3</sup> C. O. Lousto,<sup>2,3,4</sup> and R. Takahashi<sup>5</sup>

<sup>1</sup>Laboratory for High Energy Astrophysics, NASA Goddard Space Flight Center, Greenbelt, Maryland 20771

<sup>2</sup>Department of Physics and Astronomy, The University of Texas at Brownsville, Brownsville, Texas 78520

<sup>3</sup>Albert-Einstein-Institut, Max-Planck-Institut für Gravitationsphysik, Am Mühlenberg 1, D-14476 Golm, Germany

<sup>4</sup>Instituto de Astronomía y Física del Espacio-CONICET, Buenos Aires, Argentina

<sup>5</sup>Theoretical Astrophysics Center, Dk-2100 København Ø, Denmark

(Dated: October 23, 2018)

With the goal of bringing theory, particularly numerical relativity, to bear on an astrophysical problem of critical interest to gravitational wave observers we introduce a model for coalescence radiation from binary black hole systems. We build our model using the *Lazarus approach*, a technique that bridges far and close limit approaches with full numerical relativity to solve Einstein equations applied in the truly nonlinear dynamical regime. We specifically study the post-orbital radiation from a system of equal-mass non-spinning black holes, deriving waveforms which indicate strongly circularly polarized radiation of roughly 3% of the system's total energy and 12% of its total angular momentum in just a few cycles. Supporting this result we first establish the reliability of the late-time part of our model, including the numerical relativity and close-limit components, with a thorough study of waveforms from a sequence of black hole configurations varying from previously treated head-on collisions to representative target for "ISCO" data corresponding to the end of the inspiral period. We then complete our model with a simple treatment for the early part of the spacetime based on a standard family of initial data for binary black holes in circular orbit. A detailed analysis shows strong robustness in the results as the initial separation of the black holes is increased from 5.0 to 7.8 $M$  supporting our waveforms as a suitable basic description of the astrophysical radiation from this system. Finally, a simple fitting of the plunge waveforms is introduced as a first attempt to facilitate the task of analyzing data from gravitational wave detectors.

PACS numbers: 04.25.Dm, 04.25.Nx, 04.30.Db, 04.70.Bw

## I. INTRODUCTION

Black holes may be the most interesting and extraordinary objects predicted by Einstein's general relativity. Over the last forty years, a flowering of observational techniques and theoretical consideration has produced a change in perspective, bringing black holes from suspected mathematical fictions to the presumptive powerhouses behind the most energetic astronomical phenomena under study today. From quasars and Gamma Ray Bursts (GRB's) to ordinary galactic nuclei and the final state of sufficiently large stars, black holes seem now quite common astrophysical objects. The characteristic of black holes which has brought them to such prominence in astrophysics is that when they are not isolated they are emphatically *not black* but produce the most luminous astrophysical phenomena known. One can estimate that a coalescing binary system of two black holes releases energy with a peak luminosity of about  $10^{-3}c^5/G$ ,  $10^{23}$  times the power output of the Sun, during the very brief period of its merger.

These events have not yet been observed because, lacking matter, the binary black hole (BBH) system releases its energy purely in the form of gravitational waves. To the developing field of gravitational wave astronomy these are expected to be generally the brightest sources in the sky. For ground-based gravitational observatories, such as LIGO [1] and GEO600, followed shortly by VIRGO [2] and several resonant bar detectors, all sen-

sitive to "higher frequencies" in the  $10^1 - 10^3$  Hz band, the relevant coalescence events have masses on the order of large stars  $10^1 - 10^3 M_{\odot}$ . Such systems may be generated through the evolution of stellar binaries, or as recent simulations suggest through many-body interactions in globular clusters[3, 4]. Space based detectors, such as the proposed NASA-ESA LISA mission [5, 6] will be sensitive to a lower frequency band roughly  $10^{-4} - 10^0$  Hz and the relevant systems are super-massive black hole binaries involving black holes in galactic cores.

For both classes of observation, the importance of theoretical models for the expected BBH coalescence is extraordinary [7, 8]. For the current generation of ground-based interferometers beginning to take scientific data in the next few months, the anticipated signal-to-noise ratios are sufficiently small that theoretical information from BBH coalescence models may be essential to distinguishing genuine detections from noise events. For LISA, on the other hand, the signal-to-noise ratios for super-massive BBH events should be quite high, up to  $10^4$  [9]. In this case the BBH events may be so strong and numerous that the ability to make observations of other weaker sources depends on filtering out the BBH signals according to accurate model waveforms. Because the new ground-based interferometers are already beginning operations and because model information may be critical even in the developmental stages of the LISA mission, there is a pressing need for producing a fair model for the BBH coalescence immediately. As general relativis-

tic modeling techniques continue to evolve and improve, there is naturally a trade-off between the level of confidence we can have in a model and how long we wait to produce it, but the clear and present need for some kind of theoretical result, provides a strong argument against waiting. Our goal here is to introduce a practical first model which may be progressively improved as new techniques are developed. Producing coalescence waveforms from the first usable models opens up a vital channel of communication between observational and theoretical efforts that is now crucially required. Of course we expect this theoretical information to support the observational effort, providing observers with specific examples of what sort of signal they can expect. Importantly, though less widely recognized in the theoretical community, a provisional model allows observational practicalities to inform the theoretical effort. Not all theoretical concerns are equally consequential in practice, and enhanced interaction with observers through model waveforms will help to identify which details of the model need the most work.

Clearly the foundation for a theoretical model of the BBH system will be Einstein's general theory of relativity. Intensive efforts to develop numerical codes able to solve the Einstein field equations using state-of-the-art supercomputers have been underway for more than a decade now [10]. These efforts have resulted in successful studies of several phenomena but, the treatment of binary black hole systems has proven very difficult. Thus far, the full numerical treatment of these systems in three dimensions (3D), based on the traditional 3+1 decomposition of space and time, has been severely limited on one hand, because of huge computer memory and processing requirements, and, on the other, by instabilities related to the formulation of the evolution equations. These difficulties combine to cause codes to fail to be accurate before any useful gravitational wave information can be directly extracted even for sample problems such as, distorted black holes, and the so-called non-axisymmetric 'grazing collisions', where the black holes must start out yet too close to allow a clear astrophysical interpretation [11, 12] (and even for single distorted black holes [13]).

In an earlier letter [14] we presented the first theoretical estimates for the gravitational radiation waveforms and energy to be expected from the plunge of orbiting non-spinning binary black holes starting from an estimate of the innermost stable circular orbit (ISCO) as provided by Cook/Baumgarte [15, 16], using effective potential method applied to Bowen-York initial data. Such a binary system has also been considered by Buonanno and Damour [17], who produce a radiation waveform estimate without solving the full system of Einstein's equations in the (expected) nonlinear regime, but using extrapolations of the 2.5 Post-Newtonian order. In this paper we apply the *Lazarus* approach [18], to develop a functional astrophysical model for binary black hole coalescence.

A complete implementation of our approach requires at least five components. There are three basic treat-

ment regimes: (i) a Far-Limit (FL) treatment covering the earliest region of spacetime when the black holes are still relatively far apart, (ii) a Fully-Nonlinear (FN) approach to the essentially nonlinear plunge/merger region of the spacetime and (iii) a Close-Limit (CL) approach to the dynamics of the newly formed final black hole and the propagation of radiation. In addition to these are two interfaces, FL-FN and FN-CL, which require a specific means of propagating the relevant physical information from the end of one regime to the beginning of the next. Section II provides an overview of our model and a brief review of the FN, FN-CL, CL techniques which are described in detail and tested in principle in Ref. [18]. In Section III C we apply these techniques to perform a systematic study of the waveforms generated by a set of sample problems, simulations of equal mass binary black holes with no intrinsic spin starting from near the ISCO. This provides a proving ground for testing our machinery for taking initial data at the beginning of the FN regime and producing a final waveform result. The study connects to previously well-studied problems and builds up to the practical demands of our astrophysical model. with Spinning and unequal mass black holes can also be treated within our method and will be published in a different paper.

To complete the model we need to provide FL and FL-FN treatments. As our approach to this regime has not been treated extensively in Ref. [18] we provide here a more detailed exposition. In Sec. III we describe our treatment and discuss how this approach compares with other candidate treatments which might also seem appropriate concluding that based on kinematics ours is the best approach to providing modeled astrophysical data to feed into the FN part of the calculation available which is so far sufficiently developed for practical applications. But a specific advantage of having a complete model is that we can move beyond these (often dubious) kinematical arguments and explicitly study the robustness of the full dynamical model. We begin this analysis in Sec. V, with successful robustness test of the FL and FL-FN part of the model. We also extend our results to meet Post-Newtonian (PN) calculations in Sec. V D. We evolve black holes from the Post-Newtonian determined parameters for the ISCO. Section VI presents summarizes the astrophysically relevant results of our treatment for the coalescence waveforms, and provides a simple analytical approximation of our results as a practical representation for the benefit gravitational wave observers and data analysts.

## II. THE MODEL

Under the *Lazarus* approach our model is specified by providing a specific implementation for five components (FL, FL-FN, FN, FN-CL, CL). A sketch of this combined approach can be outlined by the following steps: (1) First provide description of the early dynamics of the

system with a FL approach, such as the PN method, which is appropriate for slowly moving, well-separated black holes, or some alternative quasi-stationary (QS) method. (2) Extract critical information about the late-time configuration of this system in terms of Cauchy data,  $g_{ij}$  and  $K_{ij}$ , and translate this information to a corresponding solution of the gravitational initial-value problem. (3) Apply a full 3D numerical simulation of Einstein’s equations to generate a numerical spacetime covering the non-linear interaction region. The evolution should proceed for long enough so that the subsequent evolution of the region exterior to the final single remnant black hole can be well approximated by perturbative dynamics. (4) At this point we choose a “late-time” slice from the numerically generated spacetime, extract  $\psi_4 = C_{\alpha\beta\gamma\delta} n^\alpha \bar{m}^\beta n^\gamma \bar{m}^\delta$  and  $\partial_t \psi_4$ , to quantify the deviation of the numerical spacetime from a Kerr geometry. Then (5) evolve via the Teukolsky equation, which governs the dynamics of Kerr perturbations in the time-domain [19], long enough to drive all significant radiation into the radiation zone where it can be interpreted.

For convenience in discussion we will refer to steps (3-5) through which radiation waveforms are derived from numerical simulation initial data as the “late-stage” part of the model. Likewise the “early-stage” part of the model encompasses steps (1-2) in which numerical data are produced from some model of the early part of the spacetime. A suitable implementation of the late-stage part of the model has been presented in Ref. [18]. During its development, the late-stage implementation has passed many tests, including the robustness of  $\psi_4$  and  $\partial_t \psi_4$  against nonlinear contamination of the Cauchy data [20]. In a first letter [21] our method proved to be capable of determining radiation waveforms for a model problem, the head-on collision of two black holes, with accuracy comparable to the best published 2D numerical results, allowing at the same time a more direct physical understanding of the collisions and indicating clearly when non-linear dynamics are important as the final black hole is formed. In [18] we report on internal consistency checks after including net angular momentum in the system, e.g. quadratic convergence to vanishing gravitational radiation, which our method passes, for the evolution of Kerr initial data. This is a non-trivial test of our procedure since the computed spurious radiation energy and waveforms will give us a direct measure of the ‘internal’ error with which we can determine such quantities. Typically, the levels of spurious radiation we have found for rotation parameter  $a/M = 0.8$  is around  $10^{-5}M$ .

Below, in Sec. III C we supplement these tests with a developmental study of the performance of our late-stage implementation on a series of test problems which build from the previous test problems to a fiducial case of practical interest, evolution from “ISCO” data, as described below.

In this work we will add to the model a simple treatment for the the early-stage part. We essentially model

the early part of the spacetime as a stack of spacelike slices, each slice chosen from a family of solutions of the Einstein initial value problem representing non-spinning, orbiting black holes. The solutions on the slices are further selected by kinematical (effective potential) arguments to correspond to circular orbits. This early-stage part of our model is clearly less developed than what we have implemented for the late-stage, and it is fair to note at the start that there are many reasons to pursue improvements for this part of the model. The key advantage of our present approach is that it can be applied even without further development to provide a complete provisional model which produces coalescence waveforms. It is precisely in the context of such a completed model that we have a concrete basis for evaluating any treatment of steps (1-2). In Section IV A we provide a detailed description of our treatment and introduce some relevant concerns related to this part of the model. In particular we consider the plausibility of our model in comparison with PN calculations.

One of the most attractive characteristics of the Lazarus approach is that it provides a built-in facility for cross-checking the three primary treatments underlying the model. By shifting the location of the interface regions in the model spacetime, we can effectively exchange the treatment chosen for that region of spacetime. This creates an inherent facility for validating the three evolutionary model components. We can cross-check the Close Limit perturbation theory treatment with Numerical Relativity results for the same region of spacetime, systematically incorporating a common technique for verifying both Close Limit and numerical results [13, 22, 23]. In [18] we described the basis for such comparisons via the FN-CL interface looking for phase locking and energy plateaux in the waveforms. With the addition of the early-stage treatment we can now begin to practically compare the FL and FN components of the model. Section V is dedicated to evaluating the FL model by comparison with numerical simulation. Although, the model for the FL is clearly more suspect, comparison of the results are in much better agreement than expected, validating our simple treatment as a fair provisional model.

### III. PRACTICAL TESTING OF THE LATE-STAGE MODEL

Our idea for the late-stage part of the model is to use the Lazarus tools for deriving radiation waveforms, energy and momentum radiated, plunge durations, etc, resulting from an evolution of binary black holes that have started close ‘enough’ to the location of the ISCO. We approach this case developmentally, beginning with an axisymmetric system of ISCO–separation black holes released from rest. This system has been studied extensively using 2D numerical simulations and with a previous simplified version of our model’s late-stage treatment [21]. From this head-on collision case we gradu-

ally add orbital angular momentum to the system to approach the target ISCO problem. We call this sequence of initial data sets the ‘P-sequence’ through which we vary the transverse momentum of the individual black hole from zero, in the head-on case to our target  $P = P_{ISCO}$ . The waveforms we present here are the culmination of a number of numerical simulations which were needed to establish both the effectiveness of our methodology and the plausibility of these results as a fair astrophysical model. The first two subsections lay the groundwork with a description of the particular family of initial data we are studying, and an overview of our methodology.

### A. Initial Data

The Cauchy data required to begin a 3+1 simulation of vacuum general relativity can be given in the form of a metric tensor  $g_{ij}$  on an initial spacelike and an extrinsic curvature tensor  $K_{ij}$  which contains information about how the initial hypersurface is embedded in the spacetime. The gravitational field equations include four constraints, limiting the choices for  $g_{ij}$  and  $K_{ij}$ . To present data for a binary black hole system generally requires (1) some astrophysical ansatz for plausible field configurations around (and constituting) the two black holes (2) solving the constraints.

Many conceivable approaches have been proposed and to varying degrees developed, for the case of black hole initial data. In this study we apply a variant of the best known approach, known as Bowen-York data [24]. This approach provides an ansatz for describing black hole systems through a set of restrictions on the metric  $g_{ij}$  and extrinsic  $K_{ij}$ . The assumptions are: conformal flatness  $g_{ij} = \Phi^4 \delta_{ij}$ , a maximal slice  $K_i^i = 0$ , and a purely longitudinal form for the extrinsic curvature  $K^{ij} = \Phi^{-10} (\nabla^i V^j + \nabla^j V^i - \frac{2}{3} g^{ij} \nabla_k V^k)$ . Instead of the traditional “inversion-symmetric” boundary conditions at each of the black holes, we apply a simplified variant (‘puncture’ data [25]) which allows black hole data to be represented numerically without excising the interior regions of the black holes. An advantage of this class of data is that it has been studied extensively.

A significant feature, expected to exist in the binary interaction, is the ISCO indicating the closest possible configuration of black holes at which the *conservative* part of the dynamics allow stable orbits. Although the field theory nature of the ‘Full Numerical’ approach does not lend itself naturally to a particle like description of the dynamics implicit in describing the ISCO, it is possible to construct particle-like parameterizations of appropriately chosen families of solutions to the initial value problem. In these terms, the kinematical relationships, among the solutions to the initial value problem provide a description of the system similar to the conservative particle dynamics, including an estimate for the ISCO.

Different approaches have been developed to identify quasi-circular orbital configurations and to determine the

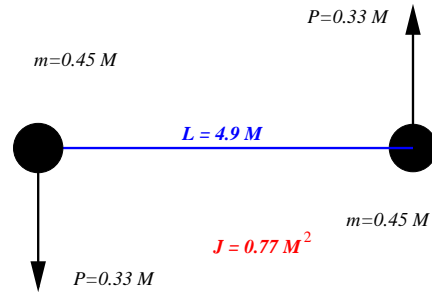


FIG. 1: Effective potential - ISCO data

location and frequency of the ISCO. We will use here the results based on the effective potential method of [15] as derived in [16] for the puncture construction of black hole initial data. This provides a space of solutions parameterized by the momenta, spins and positions of each black hole. From these solutions one can apply the Arnowitt-Deser-Misner (ADM) formalism to determine the total energy  $M_{ADM}$  for the slice of spacetime. If a bare mass is inferred for each individual black hole from its apparent horizon area, then the difference  $E_{Eff}$  can be used to identify points in the solution space corresponding to quasi-circular orbits, and ISCO.

For puncture data the ISCO is characterized by the parameters

$$\begin{aligned} L/M &= 4.9, & P/M &= 0.335, \\ J/M^2 &= 0.77, & m &= 0.45M. \end{aligned} \quad (3.1)$$

where  $m$  is the mass of each of the single black holes,  $M$  is the total ADM mass of the binary system,  $L$  is the proper distance between the apparent horizons,  $P$  is the magnitude of the linear momenta (equal but opposite and perpendicular to the line connecting the holes) and  $J$  is the total angular momentum. This configuration is represented in Fig. 1

Families of solutions to the initial value problem have been produced from other sets of assumptions on the fields as well. An approach inspired from the Kerr-Schild form of a Kerr black hole [26], provides a more natural model at least when the black holes are far apart, but has not yet been studied as a kinematical model for quasi-circular orbits and ISCO. Another treatment along the lines of the maximal/conformally flat formalism with no assumption about the longitudinality of the extrinsic curvature but with additional restrictions guaranteeing that these conditions are initially consistent with the evolution equations, is very promising but has not yet been applied to irrotational black hole systems as considered here [27, 28, 29]. Finally, an interesting first step in providing astrophysically realistic initial based PN motivated choices for the freely-specifiable portions of the data [30] will be subject of further investigation within our approach.

## B. methods

A detailed discussion of our techniques has been presented in a previous paper [18] so we only briefly review the techniques here. We first perform a numerical simulation to cover a relatively brief period of fundamentally non-linear two-body interactions to the point where the dynamics of the final black hole dominate and can be treated linearly. We then integrate the standard ADM form of Einstein’s equations using the thrice iterated Crank-Nicholson approach with maximal slicing and vanishing shift, making extensive use of the publicly available Cactus computational toolkit [31] and Brügmann’s multi-grid elliptic solver BAM for initial data and maximal slicing choices. In designing these simulations we have focused on the particular needs of our problem defined within the Lazarus approach, rather than on alternative techniques for generic applications. Some of the priorities in this case are: optimal accuracy for brief simulations in the entire region outside the final horizon, avoidance of boundary noise, and consistency with gauge assumptions applied in interfacing to the “close-limit” phase of the treatment. The accuracy requirement tends to favor the standard ADM over other approaches. Although the ADM system tends to be more susceptible to instabilities, it also tends to be more accurate before these instabilities suddenly arise.

In the cases considered here, these runs would suffer catastrophic instabilities after  $15 - 20M$  evolution, but the more critical question for our problem is that the runs be sufficiently accurate in the convergent regime prior to the instability. In some cases, other systems [32], seem to allow for significant improvements in the treatment of boundaries. But at present even these improved boundary treatments remain problematic, allowing physical wave content into the computational domain. For brief, accurate simulations it is important, and practical to move the boundary far away, causally separating it from the relevant wave-generation region. To realize this without undue computational expense we cast the initial data in specialized *fish-eye* coordinates which bring a distant outer boundary to a closer coordinate location without sacrificing physical resolution in the strong field regions [18]. Our gauge assumptions favor maximal slicing in the numerical simulations, and for simplicity without an obvious alternative, we use a vanishing shift. Other sophisticated techniques currently under development in the field, such as black hole excision, are not so relevant to our narrowly defined numerical simulation needs. We effectively excise the interior of the final event horizon when we make the transition to (purely exterior) close limit perturbation theory.

In analyzing our results we make extensive use of several special techniques. A key tool for interpreting our numerically simulated spacetimes is the complex-valued ‘ $\mathcal{S}$ -invariant’[33].

$$\mathcal{S} = 27\mathcal{J}^2/\mathcal{I}^3, \quad (3.2)$$

where  $\mathcal{I}$  and  $\mathcal{J}$  are the two complex curvature invariants  $\mathcal{I}$  and  $\mathcal{J}$ , which are essentially the square and cube of the self-dual part,  $\tilde{C}_{\alpha\beta\gamma\delta} = C_{\alpha\beta\gamma\delta} + (i/2)\epsilon_{abmn}C_{cd}^{mn}$ , of the Weyl tensor:

$$\mathcal{I} = \tilde{C}_{\alpha\beta\gamma\delta}\tilde{C}^{\alpha\beta\gamma\delta} \quad \text{and} \quad \mathcal{J} = \tilde{C}_{\alpha\beta\gamma\delta}\tilde{C}^{\gamma\delta}_{\mu\nu}\tilde{C}^{\mu\nu\alpha\beta}. \quad (3.3)$$

In vacuum general relativity this is the unique (up to rescaling) spacetime scalar quantity which can be constructed from the components of the curvature tensor which is not dominated by its fall-off behavior in an asymptotically flat spacetime. It is thus a natural tool for invariant interpretation of spacetime dynamics. A key characteristic of the  $\mathcal{S}$ -invariant which we take advantage of here is that it has the exact value,  $\mathcal{S} = 1$  in the Kerr geometry and tends to provide a useful measure of deviations from the Kerr background. As a rule of thumb, we adopt the criterion that black hole perturbation theory is likely to be effective if the real part of  $\mathcal{S}$  differs from unity by less than a factor of two (when reaching the maximum) outside of our estimated location for the horizon. In these binary black hole spacetimes, we find the maximal values of  $\mathcal{S}$  on the orbital ( $z$ ) axis.

Our most important means of evaluating the calculations is the inherent cross-checking between the two evolutionary spacetime models (close limit and numerical simulation). By changing the location of the transition between these approaches in our model spacetime, which is achieved by varying the evolution time  $T$  of the numerical simulations, we can effectively exchange one treatment for the other. If the resulting radiation is approximately unchanged, then the two independent treatments are agreeing with each other and we can be confident in the results. In practice we compare the results by separately examining the magnitude (total radiation energy  $E$ ) and phasing of the waveforms. Thus we look at the energy as a function of the transition time  $T$ , and expect to find a plateau in  $E$  once we have evolved through the most significant regions of non-linear dynamics and before the inaccuracies in the numerical simulation have grown dramatically.

## C. $P$ -Sequence results

In order to better understand the physics of the plunge we have designed a set of sequences approaching the ISCO by changing one of its physical parameters. Many different sequences are possible. The ‘ $P$ -sequence’ for which we keep the separation constant at  $L = L_{ISCO} = 4.9M$ , but vary the linear momentum,  $P/P_{ISCO} = 0, 1/3, 2/3, 5/6, 1$  is particularly interesting because it connects the well-studied case of head-on collisions from rest to our target, ISCO data. Fig. 2 illustrates the initial configurations studied with increasing linear momentum from the resting holes to the ISCO values.

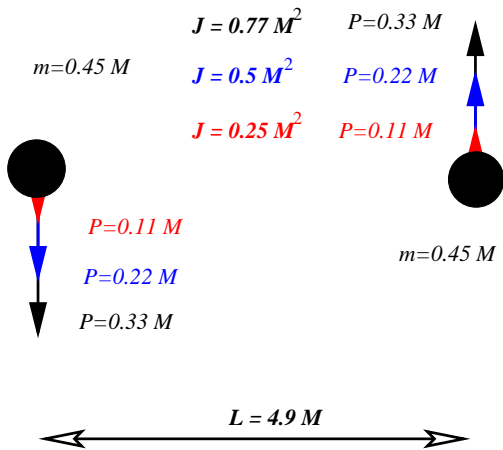


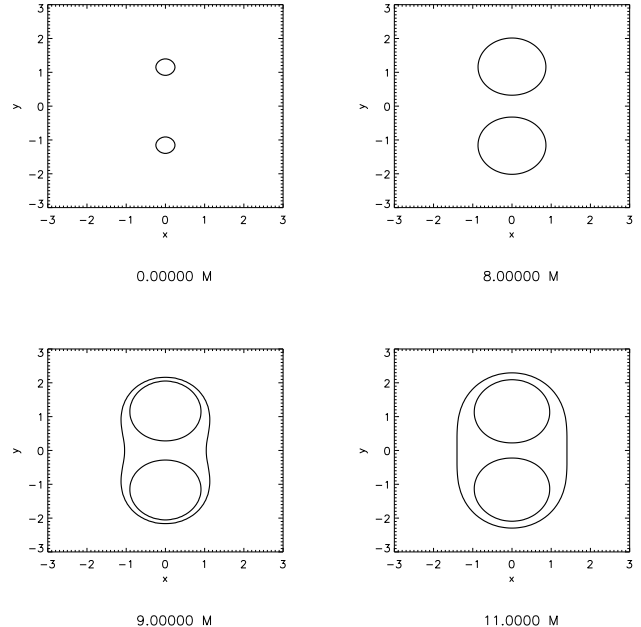
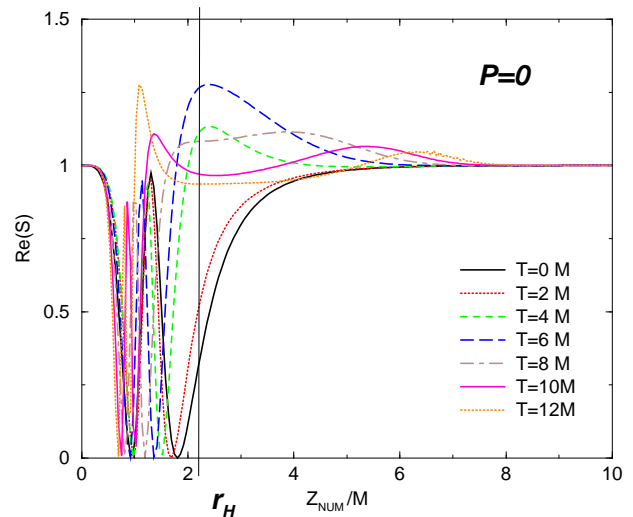
FIG. 2: Sequence P

1.  $P = 0$  (Brill-Lindquist initial data)

The head-on collision of black holes from rest has been studied using our techniques in Ref. [21] and compared with  $2D$  simulations. Here we revisit this configuration, now not with the holes lying along the  $z$ -axis, but along the  $y$ -axis, and having switched from Misner to Brill-Lindquist initial data, to serve as a reference point for the ISCO initial data. The change in orientation implies that the radiation is now predominated by  $m = \pm 2$  component, each contributing a factor  $3/8$  to the total energy; while  $m = 0$  waves have similar time dependence but smaller, contributing to  $1/4$  of the total radiated energy. Note that the reflection symmetry of the systems considered here implies that the  $m = +2$  and  $m = -2$  modes are directly related and contribute the same to the total energy radiated. Without loss of information we present only the  $m = +2$  results.

Fig. 3 shows four snapshots of the apparent horizon surfaces on the orbital plane [34]. They show that the two black holes start well detached. Clearly, the ‘grid stretching’ effect due to the vanishing shift we used during evolution makes them appear to grow in the coordinate space already after  $8M$  of full numerical evolution. These plots are particularly useful to extract qualitative information about the system. Soon after a common apparent horizon covers the system which tends to have an increasingly close to spherical shape at later times. This tends to set an upper limit on the time at which linear theory can take over as has been discussed in Ref. [18]. It is expected that a common *event* horizon should have appeared several  $M$ 's of time earlier. The key physical feature which actually makes the close limit approximation effective is that the black holes share a common potential barrier which appears even earlier than the common event horizon.

In Fig. 4 we show the time evolution (actually computed every  $1M$ ) of the ‘ $\mathcal{S}$ -invariant’. The ‘ $\mathcal{S}$ -invariant’

FIG. 3: Apparent horizons for  $P_{ID} = 0$ FIG. 4:  $\mathcal{S}$ -invariant measuring deviations from Kerr

clearly shows that space time is asymptotically Kerr ( $\mathcal{S} = 1$ ) at large distances. It also shows that the geometry at the initial slice has significant distortions near the region where the common horizon will form and hence we do not expect perturbation theory to be a good approximation at very early times. In fact we need at least  $4M$  of evolution to bring the distortions outside the horizon down the level of a factor 1.5 in the  $\mathcal{S}$ -invariant.

Fig. 5 shows the computed total radiated energy from the system using linearized theory after  $T$  of full nonlin-

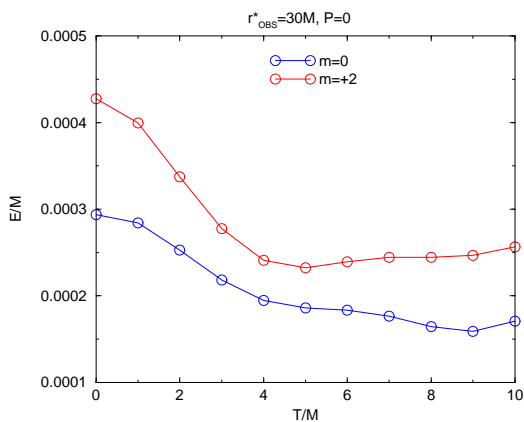


FIG. 5: Total radiated energy plots

ear numerical evolution. We see that if we insist on using perturbation theory to compute the subsequent evolution. Even at very early times, we obtain that the radiated energy varies notably for different transition times. Only when we really reach the linear regime there is a certain ‘energy plateau’. This again happens for  $T \approx 4M$  for both relevant modes  $m = 2, 0$ . Note that the curves settle down to values closely bearing the 1.5 factor among mode contributions expected for axisymmetric  $l = 2$  radiation at this orientation.

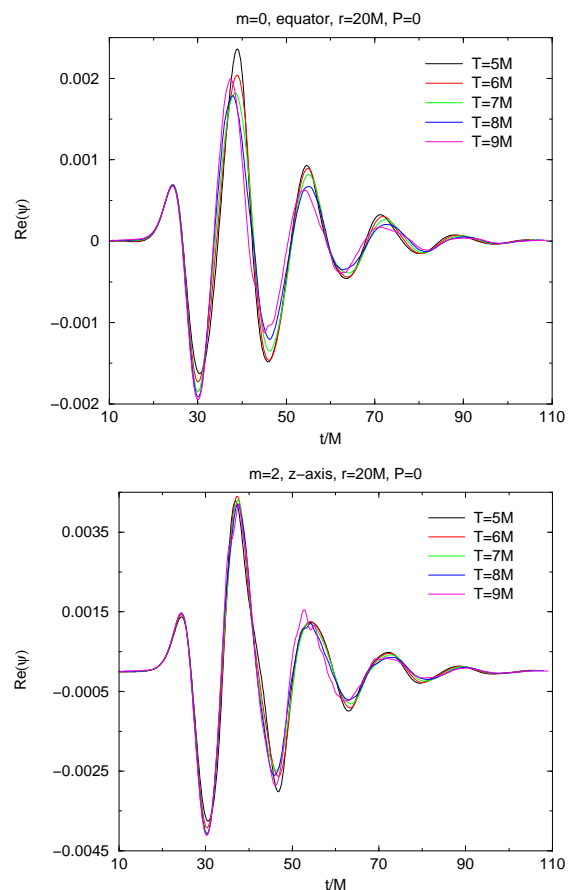
Fig. 6 displays the superposition of waveforms for the two relevant modes from  $5M$  to  $9M$  of nonlinear evolution. These waveforms are unequivocally determined once the transition time has been chosen so there are no free parameters to be adjusted in this comparison. Throughout this section we show the  $m = 0$  and  $m = 2$  waveforms for observers respectively on the equator and the  $z$ -axis, where the amplitude of each component is maximal. Specially useful, as an independent test of linearization, is the locking of the phases observed after  $5M$  of evolution. At later times we recognize the quasinormal frequency of a the final Schwarzschild black hole with a period  $\tau_{qnm} = 16.8M$ .

We observe that all the four criteria used here to determine the time this system begins to behave linearly outside the horizon coincide in setting it around  $4 - 5M$  of nonlinear evolution. Though we have not displayed it explicitly, we also find good agreement with our earlier Misner data results.

## 2. $P = P_{ISCO}/3$

Now we begin to add angular momentum to the system. In this case we give the holes an initial momentum perpendicular to the separation vector of one third of the ISCO momentum magnitude.

We show in Fig. 7 four snapshots of the apparent horizon on the orbital plane; a picture quite similar to the

FIG. 6: Waveforms for  $P_{ID} = 0$ 

head-on case, except, as expected, for a slight asymmetry along the orbital motion and the appearance of a common apparent horizon after  $9M$  of full nonlinear evolution, approximately  $1M$  later than in the head-on case. The asymmetry is a result of the orbital-like motion with respect to our vanishing shift coordinate system. The coordinate singularity (“puncture”) which must remain inside the apparent horizon is fixed in place in the grid coordinates so that the apparent horizon cannot “orbit” in these coordinates, but is, rather, stretched around in the  $\phi$ -direction. The same characteristic is evident for all our runs. This twisting of the spacetime is a generic consequence of using a vanishing shift for these simulation and illustrates the importance of using a co-rotating shift with some  $\varphi$ -component.

Fig. 8 shows the deviations from a Kerr background along the  $z$ -axis (the direction of maximal distortion) as measured by the  $\mathcal{S}$ -invariant. The picture shows clearly that at least  $4M$  of evolution are necessary to reach a perturbative regime.

In Fig. 9 we observe that the radiated energy reaches a plateau after transition times  $T \sim 4M$  consistently for both modes  $m = \pm 2, 0$ . Even for this weak radiation the approximate constancy of the radiated energy holds up

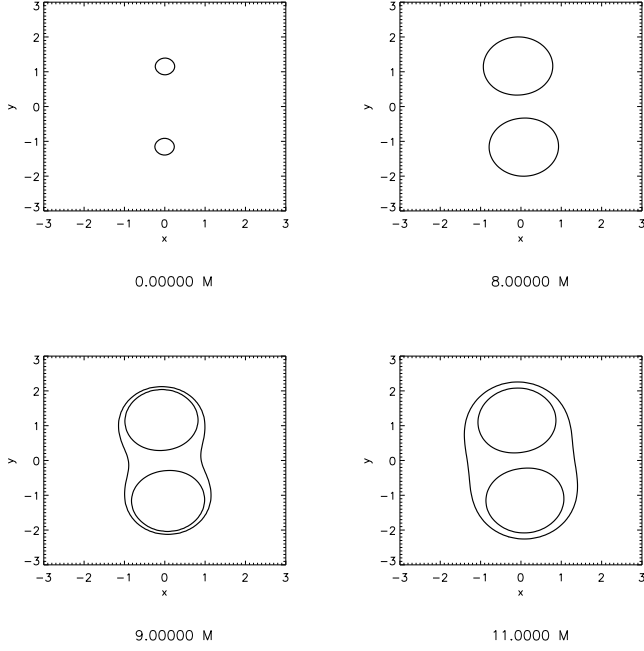
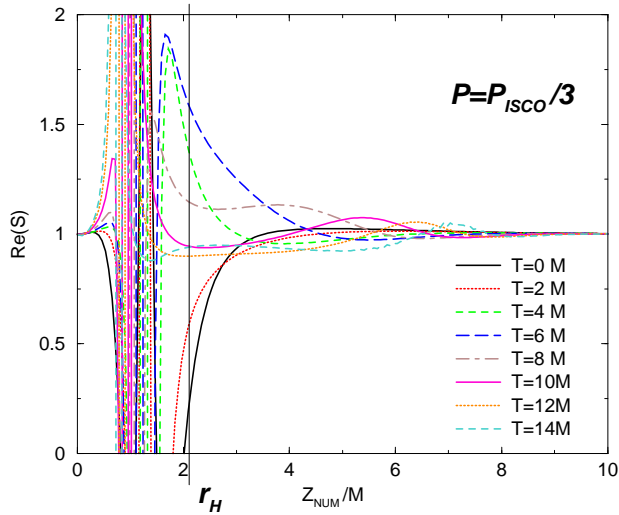
FIG. 7: Apparent horizons for  $P_{ID} = P_{ISCO}/3$ 

FIG. 8: S-invariant measuring deviations from Kerr

to  $T \sim 10M$ .

Fig. 10 displays the impressive agreement among waveforms for different extraction times and different modes. All this reached without any adjustable parameter. The frequency of the waveforms quite closely resemble those of the least damped quasinormal modes for a Kerr black hole with rotation parameter  $a/M = 0.26$ , which for  $\ell = 2, m = 2$  has a period [35]  $\tau_{qnm} \approx 15.2M$ .

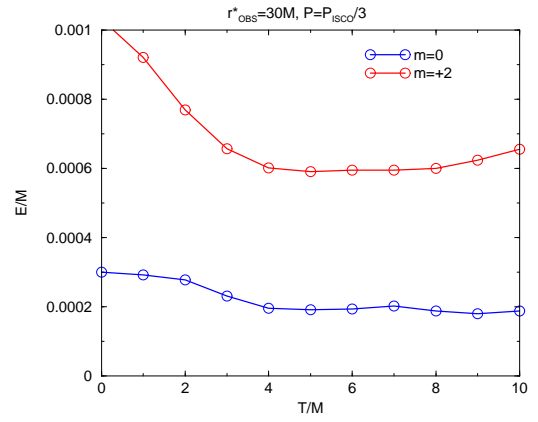
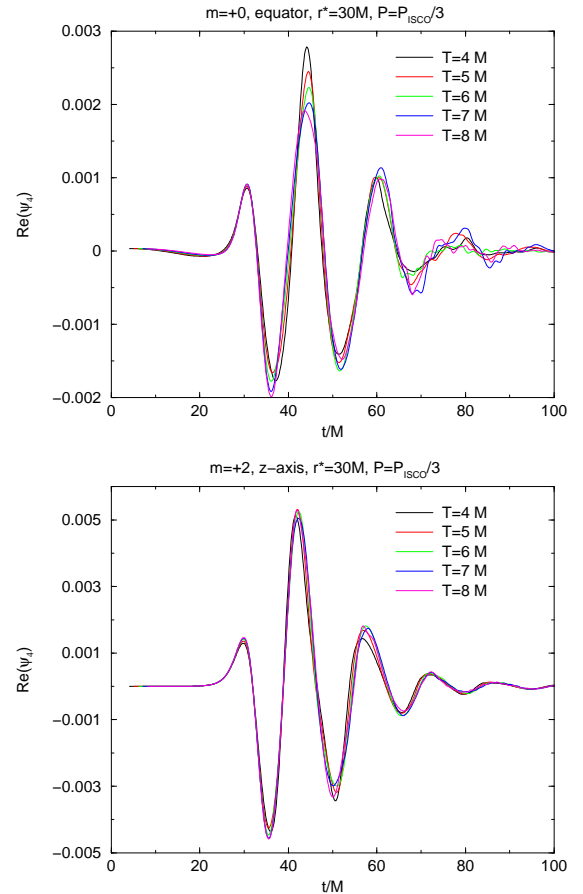


FIG. 9: Total radiated energy plots

FIG. 10: Waveforms for  $P_{ID} = P_{ISCO}/3$ 

### 3. $P = 2P_{ISCO}/3$

This case has an initial transverse linear momentum of two thirds the ISCO magnitude.

Fig. 11 displays clear effects of orbital motion deforming the apparent horizon surfaces on the equatorial plane.

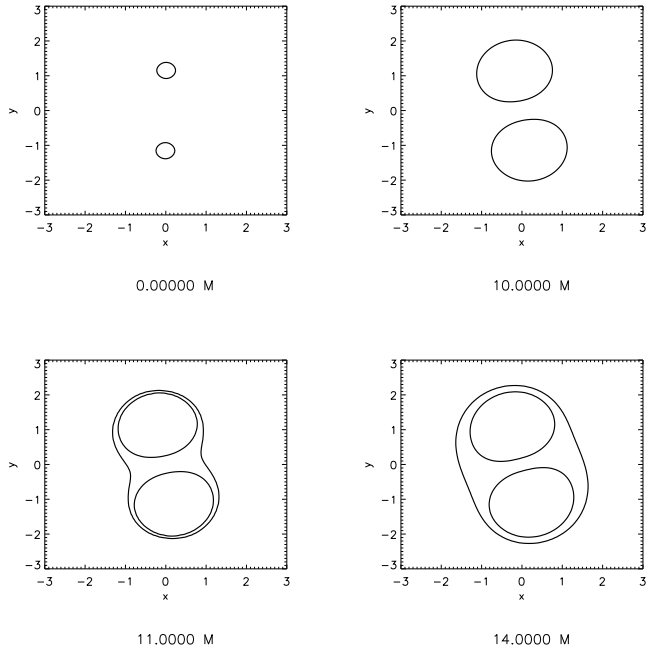
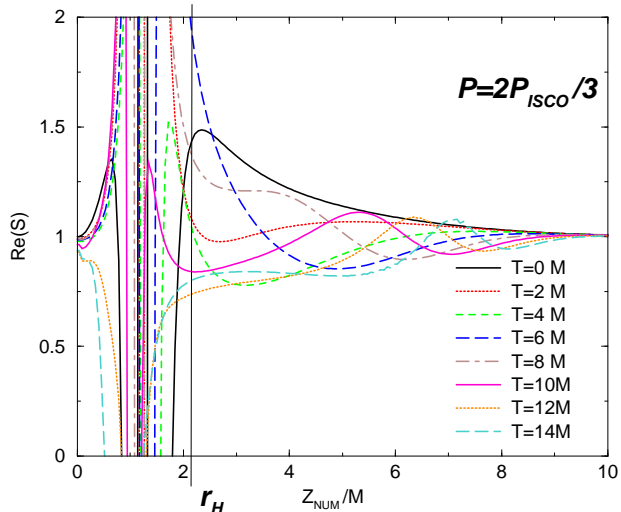
FIG. 11: Apparent horizons for  $P_{ID} = 2P_{ISCO}/3$ 

FIG. 12: S-invariant measuring deviations from Kerr

A common apparent horizon appears at  $T \sim 11M$  showing that the orbital component delays the merger of the holes into a single one as expected.

Fig. 12 shows that, consistently, the  $\mathcal{S}$ -invariant estimate for linearization is also delayed in comparison with the head-on or near head-on cases. At least  $8M$  of evolution is needed to settle down the perturbations to a small portion of the background.

Likewise Fig. 13 shows how the plateau in the energy

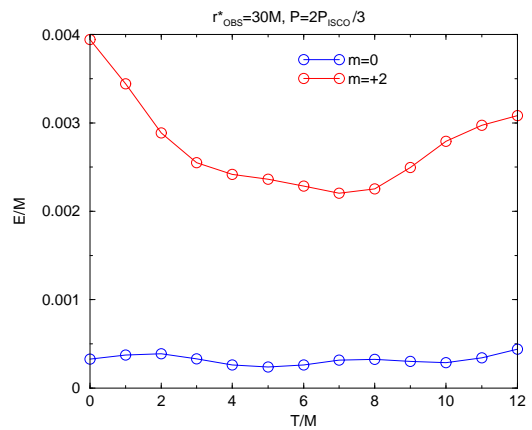
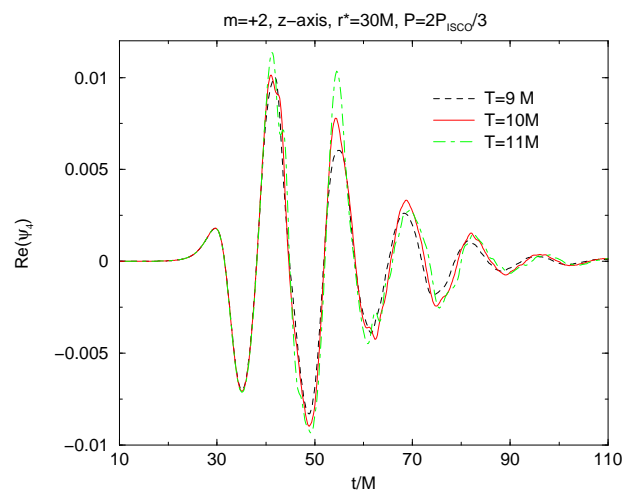


FIG. 13: Total radiated energy plots

FIG. 14: Waveforms for  $P_{ID} = 2P_{ISCO}/3$ 

is reached at later times after an oscillation around the final value. It takes  $9M - 10M$  of evolution to obtain a stable plateau.

Fig. 14 displays the leading mode,  $m = +2$ , along the  $z$ -axis with good agreement for the times where we estimate linearization takes place. Excellent phase locking is evident for the first three cycles with good agreement for the rest of the relevant signal. The frequency of the last part of the waveform agrees with the least damped quasinormal mode of a Kerr hole with rotation parameter  $a/M = 0.51$  for the mode  $m = 2$  which has a period [35] of  $\tau_{qnm} \approx 13M$ .

For the three sets of simulations just reported we have used grids of  $384^2 \times 192$  size (Making use of the symmetry along the  $z$ -axis of the problem) with a inhomogeneous distribution of the points called ‘Fish-Eye’ [18]. Each run required up to  $70Gb$  of RAM memory on a Hitachi SR-8000 at the LRZ in Garching, Germany and took about 10 hours running on 16 nodes (128 processors).

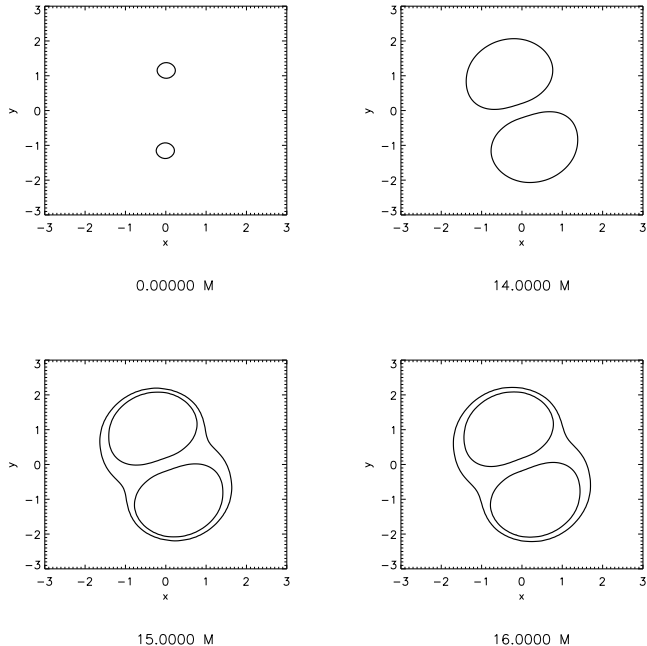
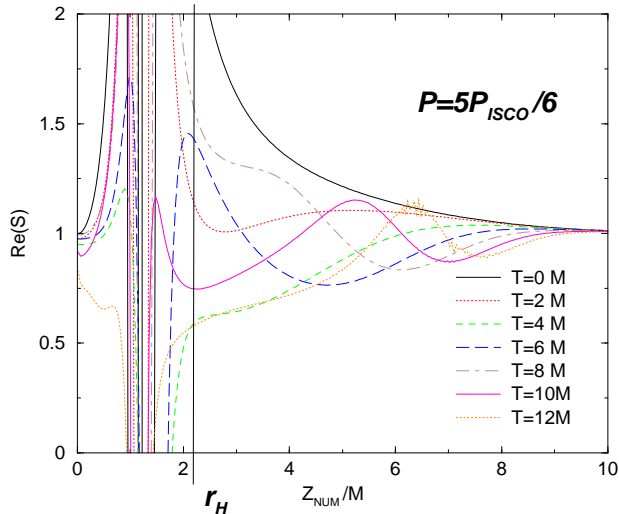
FIG. 15: Apparent horizons for  $P_{ID} = 5P_{ISCO}/6$ 

FIG. 16: S-invariant measuring deviations from Kerr

#### 4. $P = 5P_{ISCO}/6$

To closely approach the ISCO parameters we included the case of  $P = 5P_{ISCO}/6$ .

Fig. 15 shows how strongly the apparent horizon looks deformed in the grid coordinates responding to the transverse momentum. The four snapshots shows the formation of a common apparent horizon for  $T_{AH} = 14 - 15M$  of nonlinear evolution. Consistently, Fig. 16 shows the

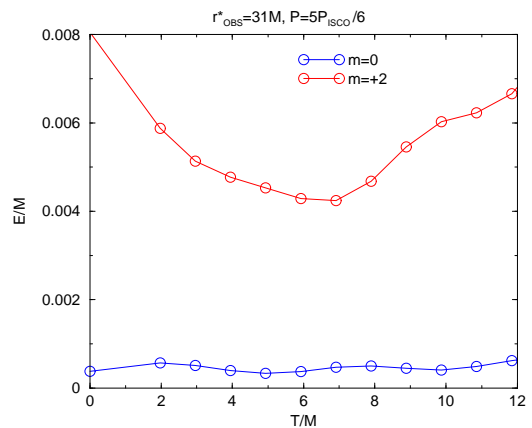


FIG. 17: Total radiated energy plots

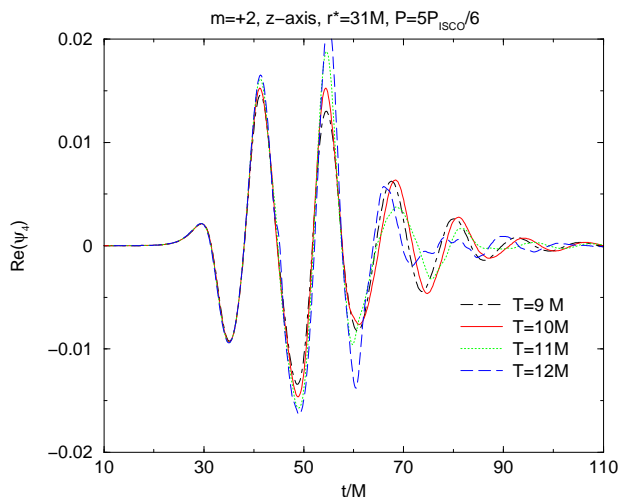
oscillations of the  $\mathcal{S}$ -invariant around the Kerr value, 1, and indicates that the linearization regime is reached after about  $9M$  of full numerical evolution. Note the stronger deformation of the initial data labeled as  $T = 0$  compared to the previous elements of the P-sequence.

A coherent picture comes from Fig. 17 which suggests that energy plateau arises after  $9M$  of nonlinear evolution, just before numerical error begins to noticeably add to the energy.. The energy radiated oscillates around the final value and is evidently dominated by the modes  $m = \pm 2$ , with very little contribution from the mode  $m = 0$  and negligible from the  $m = \pm 4$  ones. We note that adding orbital momentum in moving along this P-sequence dramatically enhances the  $m = 2$  component of the radiation with relatively little effect on the  $m = 0$  mode. Thus while the energy content of the two components was roughly comparable in the head-on case, as we approach ISCO the  $m = 2$  component is growing strongly as would be expected for a non-axisymmetric orbital system. A linear analysis [36] indicates that the leading  $\ell = 2, m = 2$  contributes to the radiated energy with a quadratic dependence in the momentum. This is precisely what we observe for small  $P$  (See Fig. 21).

Fig. 18 show excellent agreement of waveforms for different transition times in the linear regime. The phase locking is excellent up to  $t \sim 60M$ , then there seems to be some interference from spurious radiation from the boundaries of the full numerical simulation that specially affects at transition times  $T \geq 12M$ .

To compute the emitted radiation and waveforms we have made a first correction to the Kerr background to take into account the portion of the energy radiated  $\sim 1.3\%$  and the angular momentum radiated ending with a black hole with mass parameter  $M_{Kerr} \approx 0.987M_{init}$  and  $a_{Kerr} \approx 0.6M_{Kerr}$ . The normal frequency of the waveforms shown in Fig. 14 correspond quite closely to the least damped quasinormal modes of this final Kerr hole.

This simulation and the one we will report in the next

FIG. 18: Waveforms for  $P_{ID} = 5P_{ISCO}/6$ 

subsection for the ISCO have been performed on a  $512^2 \times 256$  grid requiring 10 hours of running time on 64 nodes (512 processors) of the Hitachi SR-8000 at the LRZ. The central resolution was  $M/24$  and the boundaries located at  $37M$  where the resolution reached  $\sim 1M$ .

#### D. Plunge from the ISCO data

The ISCO configuration proves to be a borderline case to study with the present full numerical technologies. We have chosen the standard ADM formulation of Einstein equations in order to ensure good accuracy during the relevant nonlinear evolution. It is known that in the ADM formulation the instabilities that kill the evolution appear suddenly and do not affect the early part of the numerical [37] integration. This is reflected in the computation of the norm of the Hamiltonian constraint,  $H$

$$L_2^{Norm} = \frac{\sqrt{\sum_{ijk} H_{ijk}^2}}{N_{ijk}}, \quad (3.4)$$

where  $N_{ijk}$  is the total number of grid points labeled by  $ijk$ , as a first measure of the numerical errors generated during the unconstrained evolution.

In Fig. 19 we show this norm for different central resolutions  $h_c$ . Even though we see the expected quadratic convergence, the exponential error growth is catastrophic and only slightly delayed by applying significantly more computational resources to increase the resolution. Eventually these runs are killed by a non-convergent instability, but the numerical errors are already a problem earlier while the code still appears to perform convergently. We take over with perturbation theory before the error has grown prohibitively.

Fig. 20 displays a detailed (every  $1M$ ) evolution of the real part of the  $\mathcal{S}$ -invariant index showing distortions

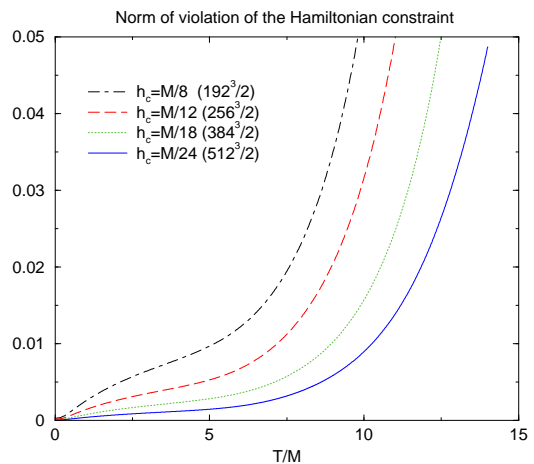
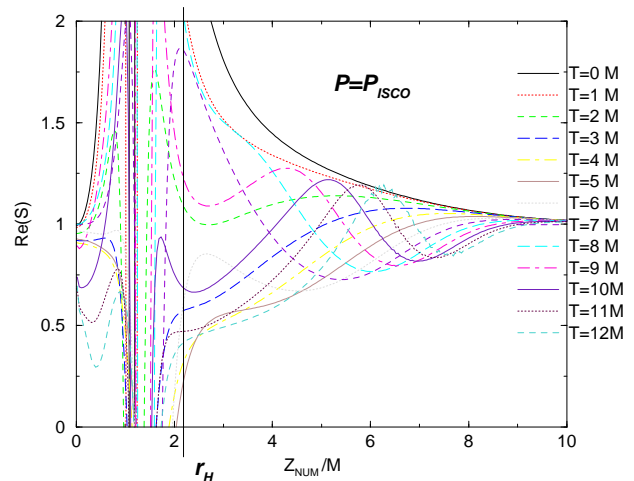


FIG. 19: Norm of the violations to the Hamiltonian constraint

FIG. 20:  $\mathcal{S}$ -invariant measuring deviations from Kerr

tions from the Kerr background (value equal 1). Initially the distortions are large and the subsequent oscillations maintain a significant amplitude near the common horizon. After the second bounce around  $T = 11M$  the distortions begin to stabilize. At larger radii a signal with relatively large amplitude begins to leave the system. This will generate the first burst of radiation coming out from the collision.

In Fig. 21 we gather the estimated linearization times for the elements of the ‘P-sequence’ and the ISCO and compare them with the time for the formation of a common apparent horizon. They seem to carry a similar dependence and off set by  $4 - 5M$  of further evolution. The offset is expected on the grounds of relating the linearization time to the applicability of the close limit approximations, associated to a common potential barrier, which appears earlier in the evolution than a common event horizon and even earlier than a common apparent horizon.

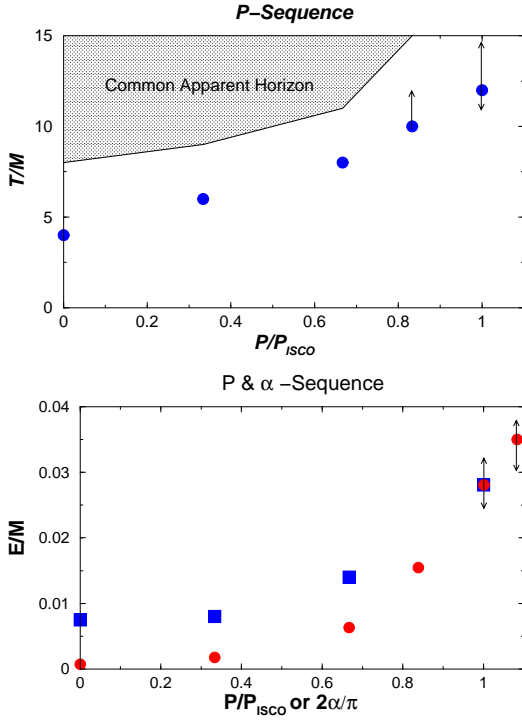


FIG. 21: Linearization time and radiated energy

We have also considered two other sequences of black hole configurations in the near-ISCO regime. The  $\alpha$ -sequence describes configurations with constant separation and magnitude of the linear momentum but varies the angle between  $\vec{P}$  and the line joining the holes. We have chosen  $\alpha = 90^\circ, 60^\circ, 30^\circ, 0^\circ$  in order to consider different radial components. As an independent test we have also studied a sequence which connects the ISCO to the close limit, (where numerical simulation should not be needed), by varying the initial separation of the holes from the ISCO separation to  $L/L_{ISCO} = 1/4, 1/8$ . For the sake of a compact description we are not going to describe those results in detail apart from reporting the radiated energy in Fig. 21. Note that the ' $\alpha$ -sequence' generates more radiation than the 'P-sequence' as expected due to its extra radial component. In this plot we also report on the case  $P = 13/12P_{ISCO}$  to check the effects of overshooting the ISCO data, finding consistent results.

To compute the total radiated energy and angular momentum radiated as a function of the transition time  $T$  displayed in Fig. 22, we have taken into account a change in the background mass  $M_{Kerr} = 0.97M_{initial}$  and the rotation parameter  $a_{Kerr} = 0.7M_{Kerr}$ . We have also considered an extrapolation of the results from two different resolutions in the convergent part of the full nonlinear simulation. In this case we find that the energy plateau is reached a little earlier (as expected if the background is closer to the actual one) and remains relatively constant from  $T = 8M$  through  $T = 11M$ .

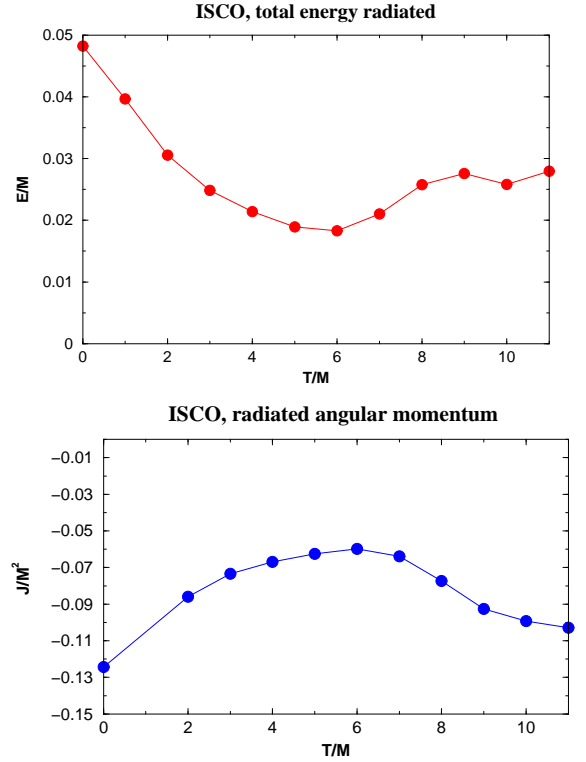


FIG. 22: Energy and angular momentum radiated

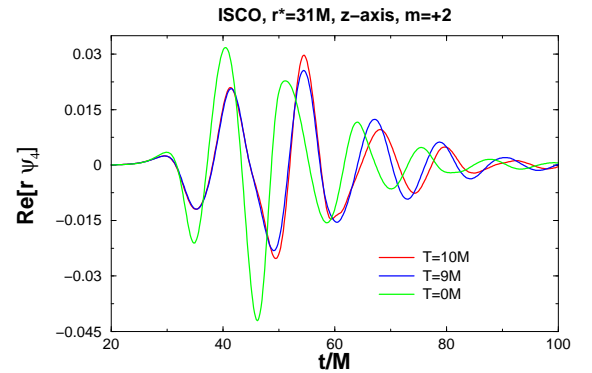


FIG. 23: ISCO Waveforms

As remarked in Ref [38] the computation of the angular momentum radiated (Eq. 5.2) is a very sensitive quantity depending on correlation of waveforms. So we can only estimate it to be around 12% of the initial momentum.

The waveforms of Fig. 23 represent our best knowledge of the plunge so far. We have included two transition times in the quasi linear regime to show the differences and as a measure of the internal errors of the method. We also display the waveform obtained if no nonlinear evolution is performed, labeled as  $T = 0M$ . The clear differences with the ones obtained in the linear regime show

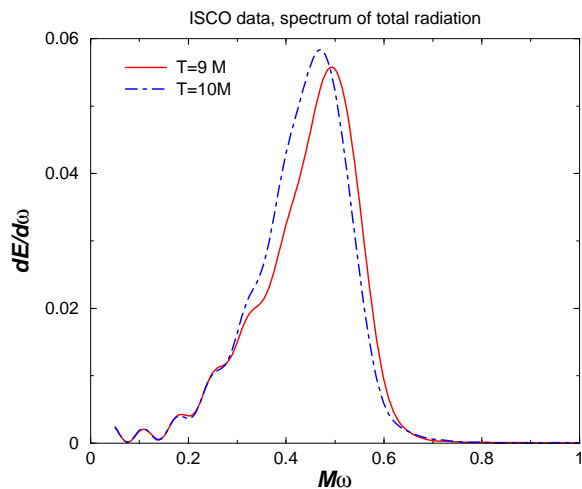


FIG. 24: ISCO spectrum

how important is to have some nonlinear evolution that settles down the system to a single rotating black hole plus distortions that will be radiated away (and down into the final black hole).

An interesting feature of the waveforms studied is that they are dominated at later times by the least damped quasinormal modes of the final Kerr black hole. For  $m = +2$  they have a period of  $\sim 12M$ . This is reflected in the spectrum of the total radiated energy, including the two polarizations and integration over all angles, presented in Fig. 24.

This spectra, again shown for different transition times to have a measure of the internal error, have a rather narrow peak at a frequency near that of the least damped quasinormal mode for a Kerr hole with  $a/M \sim 0.7$ . The lower frequency part of the spectrum is dominated by the quasinormal mode  $m = -2$  component with a period of  $\sim 19M$  that is close to the radiation-orbital frequency (one half the orbital period of the ISCO  $\sim 37M$ ). For a binary system of total mass  $M = 35M_{\odot}$  these frequencies correspond to  $475\text{Hz}$  and  $300\text{Hz}$  respectively.

### E. Critical Assessment

We have applied our late-stage model to a sequence of initial data sets ranging from the head-on collision case to the ISCO data. Having achieved the expected result in the head-on case we have slowly added orbital angular momentum. As expected the orbital motion leads to a dramatic increase in the leading  $l = 2$ ,  $m = 2$  component of the radiation, initially depending quadratically on the momentum of the system. Our study proves that some fully non-linear treatment is essential, for a reasonable treatment of the BBH system in the plunge regime. On the other hand we find also that the extent of the space-time which must be treated nonlinearly in this regime is

modest. Our estimates for the rough linearization time from our ISCO-candidate data set come to around  $10M$  of nonlinear evolution. While the overall results at the ISCO are only marginally robust, within say 20% rather than much finer precision in the head-on case, many features of the waveforms are precisely determined. The first two cycles or so, up to the peak at  $t = 50M$  or so are quite precisely determined in phase. In the worst case, that we have underestimated our linearization time, and our numerical accuracy, we would not expect dramatic changes in the early part of the waveform from an improved calculation. In many cases there are some evidently non-robust features in the later parts of the waveforms. We have traced back to several sources of error which influence this part of the waveform, most notably numerical differencing error originating near the punctures in our simulations and radiation errors associated with the finite spatial extent of our numerical domain. This study was a vital tool in our efforts to reduce finite boundary effects to the point that the overall waveform seems to be accurate within 10-20%. Because the numerical error associated with the punctures shows up predominately in the higher  $l$  parts of the waveform, it is practical to filter these effects by extracting the strongly dominant  $l = 2$  component of the radiation. This filtering preserves some 90% of the  $m = 2$  radiation energy. The filtered waveforms are much more robust, and indeed simpler to characterize (no-longer 2D). Therefore, in the subsequent analysis of our astrophysical waveform models we will focus on the  $l = 2$  radiation component.

### IV. AN EARLY-STAGE MODEL

Two important classes of treatments are applicable to binary black hole systems toward the end of the orbital epoch. In addition to ‘Full Numerical’ approaches which attempt to solve Einstein’s nonlinear gravitational field equations are PN techniques, which make perturbative expansions of Einstein’s equations in powers of  $v/c$ , and are thus most effective for describing the exterior field of slowly moving, separated binary systems.

Having established a connection to previous studies allows us confidence in our calculations as solutions of Einstein’s equations. But solving Einstein’s equations is not sufficient for work which aims to treat astrophysical phenomena. For this we need a good *model* of the system to be studied, and a method for evaluating the veracity of the model. While we continue, separately, to develop an interface between the PN method and numerical simulations which is ultimately expected to be required to provide the best astrophysical initial data, such data are not yet practical. Instead, we adopt a very basic early-stage model which takes no information directly from the PN treatment. We start our simulations with initial data derived from an alternative description black holes in quasi-circular orbit derived in Refs. [15, 16] for conformally flat black hole initial data, which we discussed

in detail in Sec. III A. As there are a variety of comparable schemes which might be applied to provide such data we also need a means to assess the “astrophysical appropriateness” of this particular scheme. Ultimately the resolution of these issues will be settled by performing a sequence of evolutions beginning with more and more separated initial systems approaching the regime where different descriptions of the initial configurations (Post-Newtonian, quasistationary relativistic ansatz, etc) merge together.

In Sec. IV A we describe such a sequence and in Sec. IV B compare our results with PN calculations applicable for well-separated systems. The comparison seems to justify our initial model as a plausible, *a priori* agreeing with PN analysis to the level of accuracy presently available. The course for future research is to refine these calculations pursuing ever improved initial models beginning the simulation earlier and earlier in the astrophysical inspiral orbital process, thereby evaluating and improving the astrophysical accuracy of these early results. In Sec. IV A we take the first few steps along this course.

### A. The QC sequence

Our “early-stage” model is composed essentially of a sequence of spacetime slices (initial data sets). We take these from the same family of solutions of the initial value equations which we have used in Sec. III, “puncture-data”, and select data corresponding approximately to black holes in circular orbit. We adapt Cook’s results, applying the effective-potential method to non-spinning black holes[15], to our case to identify a sequence of quasicircular orbits. This selection, which we call the “QC” sequence, includes data ranging in initial separation from  $5M$ , the ISCO value, to  $14M$ . Strictly speaking Cook’s results apply to a family of data determined with a different interior boundary condition than applied for our puncture-data, but the practical differences are very small. Baumgarte[16] has performed an effective potential analysis for the puncture data showing results almost identical to Cook, consistent with the noted numerical similarity of the two treatments [39]. Though not ideal, it is not true that these conformally flat initial data should completely fail to approximate an astrophysical configuration of black holes. For sufficiently well-separated binaries of non-spinning black holes the uncertainties associated with this method can be made arbitrarily small, and comparisons with post-Newtonian calculations have shown a reasonable correspondence in this limit.[15] The black hole configurations associated with our QC sequence are illustrated in Fig. 25.

Other families of initial data are available which might be applied for an alternative, similarly constructed ‘QC-sequence’, but none are as yet sufficiently developed for this application, and there is no clear way to evaluate the the various *a priori* preferences adopted in these various methods without a dynamical study, such as that of

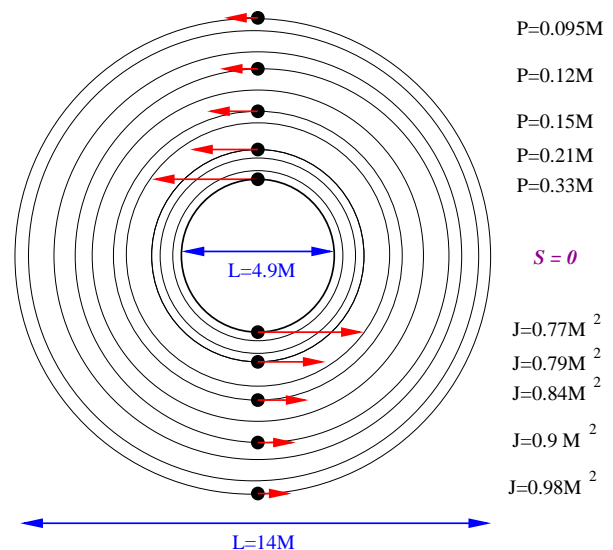


FIG. 25: Quasi-circular orbital data

TABLE I: Quasi-Circular data

Name	$L/M$	$\pm X/M$	$\pm P/M$	$J/M^2$	$M\Omega$	$m/M$
QC-B [16]	4.90	1.158	0.334	0.773	0.176	0.450
QC-0 [15]	4.99	1.169	0.333	0.779	0.168	0.453
QC-1	5.49	1.364	0.286	0.781	0.142	0.463
QC-2	5.86	1.516	0.258	0.784	0.127	0.470
QC-3	6.67	1.849	0.2148	0.794	0.1019	0.477
QC-4	7.84	2.343	0.1743	0.817	0.0760	0.483
QC-5	8.84	2.772	0.1514	0.8397	0.0612	0.487
QC-6	9.95	3.257	0.1332	0.8677	0.0497	0.489
QC-7	11.11	3.776	0.1190	0.8985	0.0408	0.492
QC-8	12.17	4.251	0.1091	0.9270	0.0348	0.494
QC-9	13.31	4.77	0.1005	0.9584	0.0297	0.496
QC-10	14.22	5.19	0.0947	0.9826	0.0267	0.498

Sec.V. With our simple model we make no attempt to contain information from the previous dynamics of the spacetime (*i.e* radiation), but attempt a fair representation of the system’s bulk motion at late times.

We have converted the QC data into actual physical parameters to be used as the initial input of the full numerical simulations. In Table I  $L$  is the proper distance between the throats of the holes,  $X$  is the coordinates of the ‘punctures’ in the conformal space,  $P$  is the individual linear momentum of the holes,  $J$  the total angular momentum of the configuration,  $\Omega$  the angular velocity as measured at infinity, and  $m$  is the bare mass of the punctures. All quantities are normalized to the total ADM mass of the system  $M$ . Baumgarte’s determination, QC-B, of the ISCO explicitly within the puncture-data family is also shown for comparison.

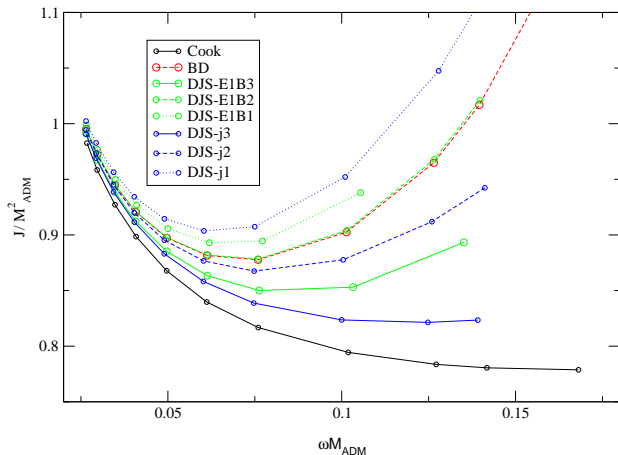


FIG. 26: The dependence of angular momentum on orbital frequency for several approaches. The results indicate that the QC sequence and ISCO is entirely consistent with the PN treatment at the level of the precision presently possible.

### B. Correspondence with Post-Newtonian parameters

In Ref. [17] Buonanno and Damour (BD) describe how to use their conservative 2PN order Hamiltonian[40] to estimate the location of the last stable orbit of a binary black hole system. In that paper they go on to evolve such systems at 2.5PN order producing an estimate for the gravitational radiation but here we are only considering the *conservative* system. Going beyond the 2PN order treatment, Damour, Jaronowski and Schäfer (DJS) have resummed the conservative part of the 3PN Hamiltonian to provide a higher-order evaluation of ISCO [41]. Until recently, the description of 3PN dynamics has been dependent on an unresolved regularization ambiguity  $\omega_s$ , but a recent dimensional regularization treatment[42] seems to fix this ambiguity with the result,  $\omega_s = 0$ . Accepting this result we can apply the methods in [41] to produce a sequence of quasi-circular orbits comparable to our QC sequence. There are two approaches to PN resummations recommended in Ref. [41]. Leaving the reader to find the details in the above references we note only that one approach, called the  $j^2$  - *method* is modeled after the resummation approach of Damour-Iyer-Sathyaprakash [43] and the other is an extension similar to the Buonanno-Damour treatment described above. The cleanest way to compare the results of these analysis is by looking at the dependence of the angular momentum  $J$  on the orbital frequency  $\omega$ , a gauge invariant comparison. In this view the minimal value in the  $J$  curves indicates the ISCO. Following DJS we have also provided the results of these treatments at the 1PN and 2PN orders

Fig. 26 provides a summary of several results. In this

plot we can assess several important considerations. The reliability of the PN treatment is accessible in two ways. The degree of convergence with higher PN order provides some indication of how much these results can be trusted. Earlier hopes that the one-body resummation approach might provide accurate waveform information up to and even beyond ISCO, possibly minimizing the need for difficult numerical treatments are not supported. The one-body approach is not converging, in the sense that the 2PN curve is everywhere closer to the 1PN curve than to the 3PN results. The  $j^2$  - *method* seems to show slow convergence for well-separated cases with small values of  $\omega$  say 0.05 or less. Likewise, there is notable sensitivity to the choice of resummation method for  $\omega < 0.06$  or so in the 2PN and 3PN cases. For the 1PN case, the one-body treatment is much closer to the higher order treatments than the 1PN results. It seems that the careful crafting of the one-body resummation method has managed to minimize the significance of 2PN terms for close agreement between the 1PN and 2PN results, but this treatment has not been done as much for the heretofore unknown dependence on the higher PN order terms, thus producing the appearance of anti-convergence in the one-body resummed PN sequence.

Comparing the post-Newtonian sequences with our QC sequence it is notable that the PN results uniformly approach the QC sequence with increasing PN order. Surely the limit of the PN sequence curves approaches something other than the QC curve, but no difference between our curve and the apparent limit of the PN sequences is yet discernible at 3PN order. Consistently the location of ISCO estimated by the PN treatments approaches the parameters of the effective potential ISCO data we used to the level of precision at 3PN. This analysis suggests that the parameters of our ISCO are at least as dependable as those given at 3PN and in fact entirely consistent with the PN sequence to the degree of precision currently possible. The PN results suggest that  $\omega_{ISCO} \geq 0.075$  but do not provide a clear upper bound.

Going beyond the comparison of the invariants  $J$  and  $\omega$ , we can make comparisons in gauge. The ADM gauge applied in the one-body approach is a directly generalization of the isotropic coordinates applicable to conformally flat data. We can thus compare the separation dependence directly for the one-body treatments and QC sequence. (The gauge transformation for the  $j^2$ -method is impractical.) The comparison in Fig. 27 shows profound agreement among all treatments all orders for separations  $r_{ADM} > 4M_{ADM}$ . For closer separation the PN gauge transformation begins to fail (cannot be solved) in some cases. The other relevant quantity is the effective potential  $E = (1 - M_{rest}/M_{ADM})/\nu$  shown in Fig. 28. The results are consistent with the conclusions from the  $J$ - $\omega$  comparison.

It is worth remarking here that the above agreement is also consistent with some recent results using the standard 3PN expansion in the standard Taylor form, without using resummation techniques [44].

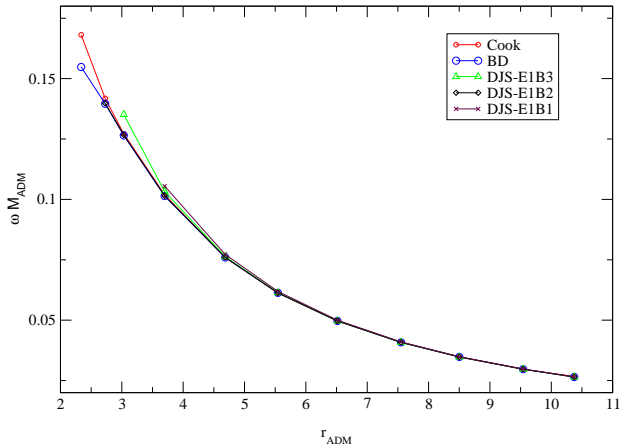


FIG. 27: The dependence of orbital frequency on ADM-gauge separation shows remarkable agreement among all cases.

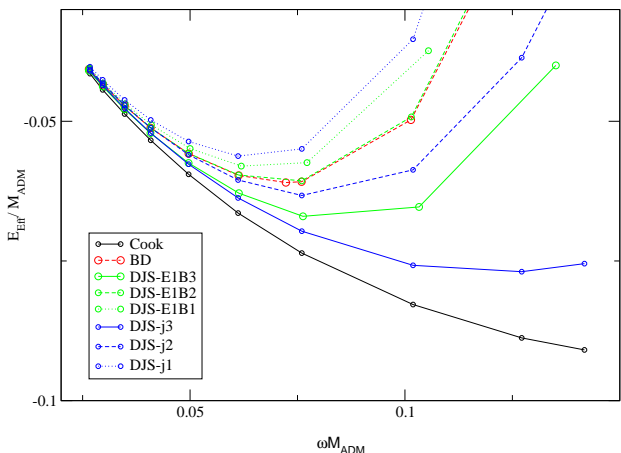


FIG. 28: The dependence of the effective potential  $E_{Eff}$  on orbital frequency for several approaches is consistent with the results for angular momentum shown in Fig. 26

## V. ANALYZING AND TESTING THE FULL MODEL

A fundamental feature of the Lazarus approach for binary black hole spacetimes is that have simultaneously at hand alternative approaches applicable to the interface regions of our model spacetime. We have extensively demonstrated how we can take advantage of this feature at the FN-CL interface to cross-check the results of the CL and FN treatments against each other, and indeed to better understand the physics of the spacetime. Even with our very simple model for the early-part of the spacetime we can begin applying the same type of test at the FL-FN interface.

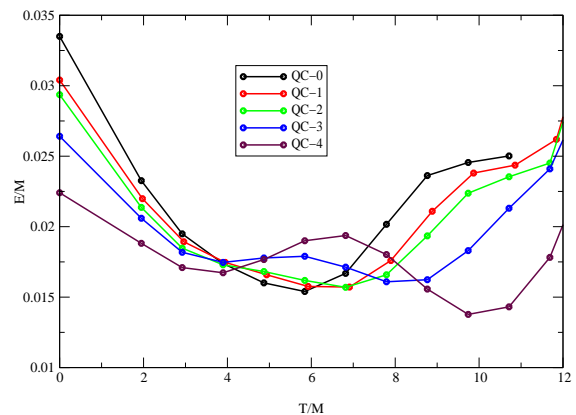


FIG. 29: Radiated energy for the QC-sequence.

The principle is the same, now, instead of altering the time of transition from FN to CL we alter the time of transition from FL to FN, and compare the resulting waveforms. In practice this means we select alternative data sets from the QC sequence and compare the waveforms. If our model is astrophysically reliable, then the shape of our waveforms should be independent of variations in the choice of QC-sequence data set (labeled by a QC-number). In this section we will compare the waveforms generated over a broad range of the QC sequence, treating the cases ranging from QC-0 to QC-4 with initial proper separations ranging from about 5.0M to about 7.8M. In each case we find a total radiation energy of about 2.5-3%M during the course of the burst. As described in Sec. III B, we look for a plateau in the dependence of the total radiated energy on the FN-CL transition time  $T$ , shown here in Fig. 29. The several methods described in Sec. III B collectively suggest linearization time of around  $T \sim 9-10, 10-11, 10-11, 11-12, 13-14M$  respectively for case QC-0 through QC-4. In all cases numerical inaccuracies begin to affect our results in the vicinity of  $T = 12-13M$  as is apparent in the figure so the later case, especially QC-4 are only very marginally linearized before numerical problems are significant. As is discussed in more detail below, we find that significant amounts of angular momentum are radiated away. For the lower separation cases, QC-0 – QC-2 roughly  $.10 - .11M^2$  of the angular momentum is lost, enough to significantly alter the value of the close-limit background black hole spin parameter  $a$ , so for the results presented in this section we have set the background black hole angular momentum to the value given in Table I minus  $0.11M^2$ . [47] Likewise we reduce the background mass to  $M = 0.974$ .

As our simple early-stage model has less structure than the late-stage part, we have a slightly weaker comparison to make between the two treatments. In Sec. III C we had *no freedom* in our waveform superposition comparison. Now, for the earlier transition, the shape of the

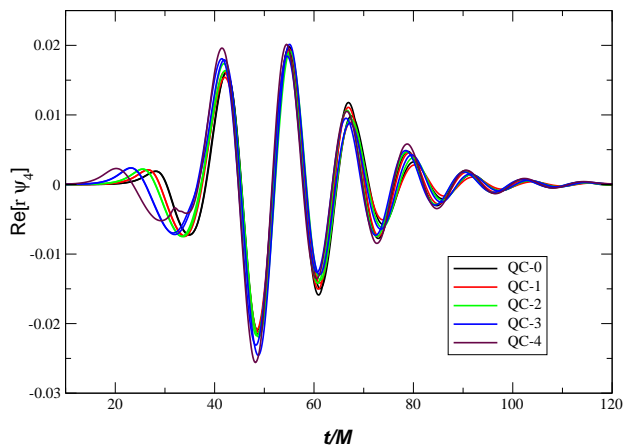


FIG. 30: Real-part of QC-sequence waveforms for the  $\ell = 2$  multipole. This plot compares ten waveforms including in the FN-CL transition time  $T$  as well as variations in the QC-sequence from QC-0 to QC-4 ( $L = 5.0M$  to  $L = 7.8M$ ). The agreement over a broad range of model parameters provides support for the fidelity of our astrophysical model.

waveform is still fully constrained, but the overall phase–or time–lag between different waveforms is free because our simple early-stage model doesn’t include any information about the time and rotational offsets between the various QC sequence slices as they are rigidly embedded in the “astrophysical” spacetime. We will have to set this by hand from the waveforms.

As motivated in Sec. III C, we will filter all the waveforms considered here to take only the  $l = 2$  part. This has the effect of efficiently eliminating of the higher angular frequency noise generated in the numerical simulations, while preserving practically all the physical radiation. Also, restricting to the  $l = 2, m = 2$  part of the radiation as the overwhelmingly predominant component completely specifies the angular dependence so that we can, without loss of generality, focus on the radiation projected toward an observer on the positive  $z$ -axis.

On the basis of the waveform’s phase, a good fit results from shifting the time-axis by 0.0, -1.6, -2.9, -5.1, and -8.0 for the QC-0 through QC-4 waveforms, respectively. The results are shown in Fig. 30. Table II reports those values for approximate linearization times corresponding to the FN-CL transition. One can interpret the phase-shifts as a measure of the differential orbital-plunging times for the elements of the QC sequence.

The remarkable agreement among ‘QC’ waveforms is the result of certainly an appropriate combination of orbital parameters  $X$  and  $P$ . Note that if we keep  $X$  fixed and change  $P$ , like in the ‘P-sequence’, the waveforms do not superpose, and if we choose similar  $P$  and different initial separations  $X$ , like comparing the waveforms of  $P = 2P_{ISCO}/3$  and QC-3 (see Figs. 14-30) or  $P = 5P_{ISCO}/6$  and QC-1 (see Figs. 18-30) we do not find any superposition of amplitudes nor phases.

TABLE II: off set shift  $t \rightarrow (t - t_0)$

Name	$L/M$	$t_0/M$	$T/M$
QC-0	5.0	0.0	9-10
QC-1	5.5	1.6	10-11
QC-2	5.9	2.9	10-11
QC-3	6.7	5.1	11-12
QC-4	7.8	8.0	13

It is also notable that there seems to be a pretty smooth transition from inspiral to plunge. This suggests that it will be hard to make a sharp definition of the ISCO, but our results compared with those of the Post-Newtonian [42, 45] approximation and that of Grandclement et al. [27] seems to indicate that starting from QC-3 or QC-4 data produces a good approximation to the plunge.

The striking agreement seen in Fig. 30 clearly supports the notion that these different initial data sets correspond approximately to the slices of a single astrophysical spacetime. In fact the agreement far exceeds what anyone would have expected from this family of conformally flat initial data sets, widely regarded on the basis of a *a priori* kinematical analysis as needing to be improved upon before any astrophysically meaningful results might be obtained. Whatever the difficulties are with these data, they do not strongly affect the resulting waveforms.

### A. Polarization

We observe an interesting correlation of the two polarizations of the waveforms here represented by the real and imaginary parts of  $r\psi_4$  along the  $z$ -axis. Except at early times, they are pretty much 90 degrees out of phase. The condition corresponds to circular polarization, as can be seen more directly if we consider our complex-valued waveforms in the representation  $\psi_4(t) = A(t)e^{i\varphi t}$ . Physically this describes the wave according to an instantaneous magnitude  $A$  and a polarization angle  $\varphi$ . Fig. 31 shows the time dependence of the polarization angle for one of our waveform cases, QC-3. After some complicated initial undulations (after around 40M, recall that the observer is located at  $r^* \approx 30M$ ) the polarization angle grows smoothly indicating circular polarization. Fig. 32 shows the instantaneous magnitude of the wave, independent of the polarization angle. For circular polarization the magnitude does not vary at the radiation frequency, but more slowly. The figure compares wave magnitude for the QC-sequence cases. At early times, the wave is not circularly polarized, and the magnitude oscillates strongly before becoming dominated by the non-oscillating (circularly polarized) component. The curves in the figure have been translated by the same time-shift applied in Fig. 30 above to get phase agreement in the waveforms. The arched circularly-polarized late-time

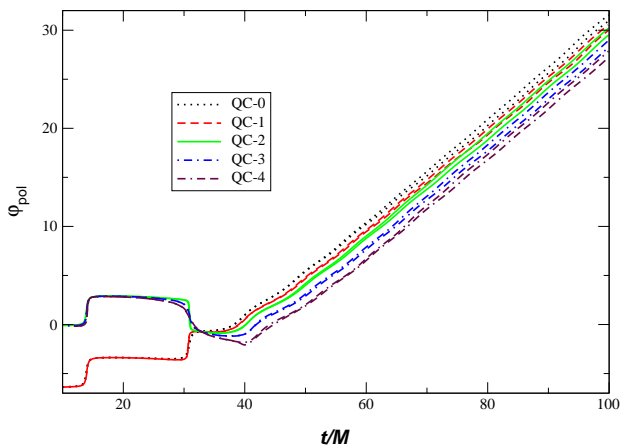


FIG. 31: Polarization angle. For all QC-sequence cases the radiation is predominantly circularly polarized after an early period of initial-data dependent fluctuations. The colors are as labeled in Fig. 29. The curves have been offset if time as

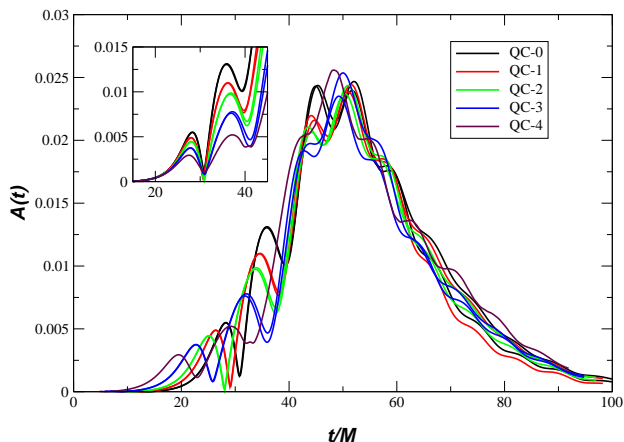


FIG. 32: Instantaneous radiation magnitude, independent of polarization angle. The colors are as labeled in Fig. 29. The inset shows the early part with time set to zero at the start of numerical evolution.

parts of these roughly superpose after this time-shift, but the oscillatory part, shown without the time offset in the inset, is timed to the initial data, and varies notably as we change among the different data sets. This suggests that the non-circularly-polarized part of the waveform is predominantly an initial-data artifact. Notably also, this non-astrophysical artifact component seems to shrink for the cases of initially more separated systems, as expected since the astrophysical interpretation of the initial data is not problematic in the limit of well-separated black holes, reproducing two Schwarzschild black holes with a small boost.

The physical interpretation of this polarization effect is that the system’s dynamics are dominated throughout the interaction by rotational motion. Even during the “ringing” of the final black hole, the perturbations seem

to circulate around the black hole rather than the bell-like ringing, one might naively expect.

We remind the reader that this discussion of waveforms is focused on the appearance of the radiation to distant observers on the system’s rotational axis. For observers in other locations the polarization will generally be elliptical, but conforming to a simple pattern consistent with the circular motion of the source. In the equatorial plane the observer “sees” no circulation in the source and the radiation reduces to “+” polarization. Moving around toward the negative z-axis, the observed radiation approaches circular polarization of the opposite orientation.

## B. Radiated Energy and Angular Momentum

The total radiated energy  $E$  and angular momentum  $J$  at infinity per unit time ( $u = t - r^*$ ) are computed as in Ref. [38],

$$\frac{dE}{du} = \lim_{r \rightarrow \infty} \left\{ \frac{r^2}{4\pi} \int_{\Omega} d\Omega \left| \int_{-\infty}^u d\tilde{u} \psi_4(\tilde{u}, r, \theta, \varphi) \right|^2 \right\} \quad (5.1)$$

$$\begin{aligned} \frac{dJ_z}{du} = & - \lim_{r \rightarrow \infty} \left\{ \frac{r^2}{4\pi} \text{Re} \left[ \int_{\Omega} d\Omega \left( \partial_{\varphi} \int_{-\infty}^u d\tilde{u} \psi_4(\tilde{u}, r, \theta, \varphi) \right) \right. \right. \\ & \left. \left. \times \left( \int_{-\infty}^u d\tilde{u}' \int_{-\infty}^{u'} d\tilde{u} \bar{\psi}_4(\tilde{u}, r, \theta, \varphi) \right) \right] \right\}. \quad (5.2) \end{aligned}$$

where  $d\Omega = \sin \theta d\theta d\varphi$ .

If we consider the magnitude and polarization angle representation of  $h$  as in Eq. (5.3), *i.e.*  $2 \int \int \psi_4 = A(t) e^{i\varphi(t)}$  then we find that radiation energy is generated both by time dependence in the magnitude  $A$  and the polarization angle, but angular momentum flux is generated only by the rotation of the polarization vector. Thus we can expect to approach maximally efficient radiation of angular momentum  $dJ = m/\omega dE$  [19] for the case of circular polarization. This is perhaps the most important consequence of the circular polarization pattern which we observe in our radiation. Note that, for our case the most significant radiation has  $m = 2$  azimuthal dependence with a frequency near  $\omega \sim 0.5$  so that we can expect  $dJ \sim 4M dE$ .

## C. Memory

Up to this point we have studied the radiation as represented by  $\psi_4$ , which is related to the second time derivative of the usual metric disturbance waveform components  $h_+$  and  $h_{\times}$  by [19]

$$h_+ - ih_{\times} = 2 \lim_{r \rightarrow \infty} \int_0^t dt' \int_0^{t'} dt'' \psi_4. \quad (5.3)$$

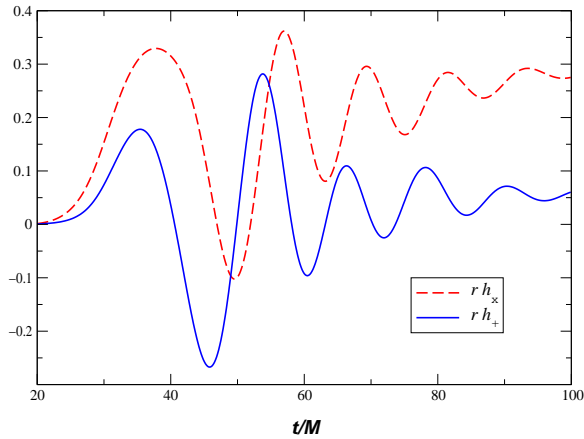


FIG. 33:  $rh_+$  and  $rh_x$  for QC-3 with trivial integration constants.

Physically our waveforms correspond to the tidal acceleration of neighboring observers (or mirrors perhaps). Naturally we can integrate to get their relative velocities and displacements, but this presents us with a problem: How do we set the integration constants corresponding to the initial displacements and relative velocities of our neighboring observers? A burst of radiation which allows initially quiescent observers to return to their original resting places is described as a “normal” burst, otherwise it is called a “burst with memory.” In trying to integrate our waveforms we find that observers at rest when our wave arrives will not return to their original resting positions, and seem not to return to rest at all. The result of direct integration of our waveforms is shown in Fig. 33 for a typical case, QC-3.

The figure shows a strong memory effect for  $h_x$  and a much weaker effect for  $h_+$ . The  $h_x$  effect is very robust with respect to the QC-sequence, while the  $h_+$  memory effect may increase slightly with initial separation, but this is not clear. Does this mean then that colliding black holes, contrary to expectation, produce a burst with memory? Not necessarily. Our wave is only the last part of a much longer wavetrain. Let us adopt the hypothesis that the full wave train is a “normal” burst, and consider whether our results contradict the hypothesis. A key point is that neighboring observers of the full wavetrain, which were initially quiescent, will not be at rest in the middle of the wavetrain, *where our wave starts*. By hypothesis, we expect these observers to return to relative rest so we must expect a change in their relative velocities and positions through the passing of our part of the wave. Our results are consistent with the hypothesis of finally resting observers if the “cross” observers, separated transversely by  $\Delta L$  at a distance  $R$  from the binary system, are initially moving with speed  $v \sim 0.0014\Delta L/R$  and the “plus” observers are initially displaced by about  $0.02\Delta L M/R$ . From the quadrupole formula for two orbiting point masses positioned instan-

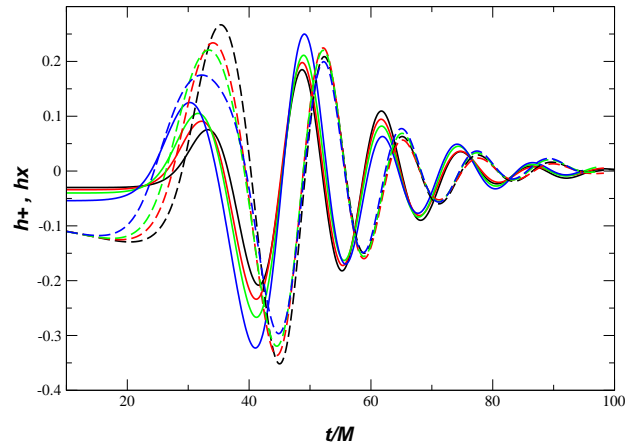


FIG. 34:  $rh_+$  and  $rh_x$  with integration constants set to fit “normal burst hypothesis”. Solid curves are ‘+’ polarization. Dotted curves are cross polarization.

taneously on the y-axis as our black holes are initially we expect that the cross observers will be moving with an initial velocity of  $2\Omega A$  and the plus observers will be initially displaced by  $A$  where  $\Omega$  is the orbital velocity and  $A$  is the momentary amplitude of the radiation. Our results are then consistent, at an order of magnitude level with what might be expected from extrapolated post-Newtonian results as presented in [46]. At present it would be inappropriate to pursue this quantitative relationship too far since there may be subtle effects, such as transients in the early parts of our waveforms or frame dragging of the radiation. In the end, our memory effect is plausibly consistent with the “normal” burst hypothesis. But this is certainly an interesting area for further study.

If we provisionally adopt the normal burst hypothesis, it is then most reasonable to perform the integrations required in Figure 33 with the integration constants set such that the strains approach zero at the end of the burst. Because our waves are not completely quiescent and prone to small errors in the late time region, some visual judgment is required in choosing appropriate integration constants. After shifting the time as above, we get reasonable waveforms upon offsetting the  $h_+$  curves by 0.015, 0.017, 0.020 and 0.027 respectively for the cases QC-0 through QC-3 in the second integral only. For  $h_x$  we offset by  $h_x \rightarrow h_x - 0.002 \times t - 0.009$ . The resulting waveforms are shown in Fig. 34. Unlike the other plots in this section we have included only one curve for each polarization from each QC data set. It is interesting to compare these “strain” waveforms with the other “acceleration” waveforms presented so far in this paper. An obvious difference is that the sharp growth in amplitude during the burst, seen in Fig. 32 for instance, is greatly muted here. The stronger growth in the  $\psi_4$  waveforms is a consequence of the two factors of  $\omega$ , which is rapidly

TABLE III: 3PN-E1B-ISCO data

Name	$L/M$	$\pm X/M$	$\pm P/M$	$J/M^2$	$M\omega$	$m/M$
3PN-E1B	$\sim 7.3$	2.119	0.200	0.8476	$\sim 0.085$	0.469

increasing, obtained from two time derivatives. A consequence of this evident in the figure is that the peak in amplitude comes earlier in the strain waveforms, pushing back to around,  $T = 40M$  near the beginning of the astrophysically credible part of the waveform. In the early time region the figure suggests that the large QC cases are tending toward longer wavelength early waveform, as one would hope to see when beginning with “astrophysically earlier” data. Finally we note that phase relation between the two polarizations, which we have attributed to circular polarization is not disrupted by two time integrations, and is equally evident in the strain waveforms.

#### D. Comparison with Post-Newtonian results

As a point of comparison we also consider the 3PN ISCO determined by the method of the effective one body (E1B) of Ref. [42] and obtain the parameters (in the ADM gauge) given in table III. Note that in Ref. [44] it was stressed the fact that to third post-Newtonian order is not obvious that the one body resummation is better than the ‘bare’ results. In this case we find that the ISCO so determined have parameter very close to the  $QC - 2$  case studied here.

In order to quantify the gravitational radiation generated during this plunge we use this 3PN ISCO parameters to evolve Bowen-York initial data. The resulting waveform is plotted in Fig. 35 and compared with the QC-3 and QC-4 cases, showing closer agreement with the QC-3 waveform.

For the full nonlinear part of the simulation we have used a nonuniform grid of  $512^2 \times 256$  and  $448^2 \times 224$  with boundaries at  $37M$ . We have also considered different nonuniform grids and boundary locations on another  $512^2 \times 256$  simulation to check the robustness of the results. The largest runs lasted for 10 clock wall hours on the 64 nodes of the SR-8000 Hitachi computer at the LRZ and used up to 170Gb of RAM memory.

The analysis of the PN determination of the ISCO shows that its separation and linear momentum parameters are close to those of the case QC-3. In retrospective, as we have seen, the plunge waveform does not dramatically change for the five cases studied, i.e. QC-0 to QC-4, hence our predictions for the plunge waveforms are compatible with the third Post-Newtonian order orbital parameters for the ISCO as well.

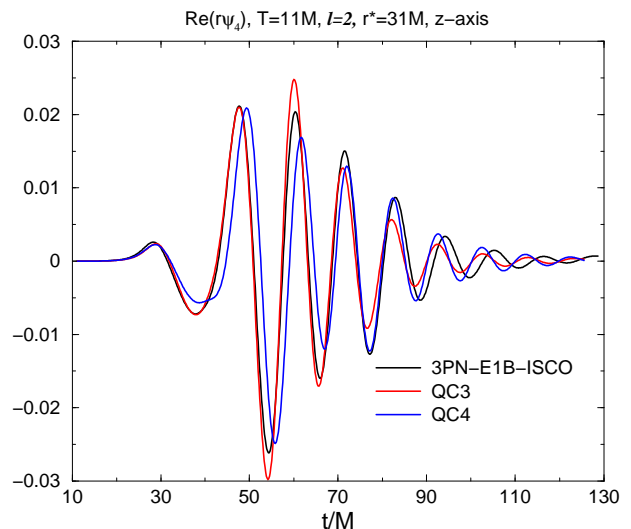


FIG. 35: Comparisons of Waveforms 3PN, QC-3, QC-4 Waveforms

## VI. SUMMARY OF ASTROPHYSICAL RESULTS

In the last section we have presented a detailed analysis of resulting waveforms from our model for the final plunge of a system of equal-mass, non-spinning (irrotational), non-elliptically orbiting binary black holes. The domain of astrophysical validity waveform is limited to the time from right around the first burst peak forward but the surprisingly lack of internal model-dependence in our results suggests that we can be confident (say to the level of 20%) in our description of the final radiation burst from such a system. We find these results convincing enough to merit their adoption, among interested researchers, as a provisional description for relevant astrophysical work, such as in the development of strategies for observation of gravitational waves. As it has been emphasized that any new information may be very valuable for improving the efficiency of gravitational wave search algorithms [7], and for the interest of readers not yet immersed in the effort to model relativistic systems we briefly review the results from a more applied astrophysical viewpoint.

Our waveforms cover the final few cycles of gravitational radiation from the peak onward. Within about four cycles the signal is reduced to only a few percent of its peak value. In geometric units this takes about  $50M$ , which corresponds, for a  $20M_\odot$  system to about  $0.1ms$  or, for a  $10^6M_\odot$  system of supermassive black holes about one minute. During this brief time vast amounts of energy are released, equivalent to about 2.5-3% of the system’s total mass and  $\sim 12\%$  of its angular momentum. The peak gravitational wave luminosity is about  $0.0015c^5/G$  or about  $5 \times 10^{56} ergs/s$ . The radiation is strongly polarized in the same manner as expected from

a rotating gravitational source with circular polarization for radiation propagating along the rotational axes and “+” polarization for radiation in the equatorial plane. As generally expected the radiation is predominated by an  $l = 2, m = 2, s = -2$  spin-weighted spherical harmonic angular distribution so that that the intensity is 16 times greater along the axes than in the equatorial plane.

The simple appearance of our waveforms, as shown in Fig. 30 suggests that rather than asking for awkward numerical data files, other researchers may benefit from a straightforward analytic fitting of our result with essentially the full information at our level of confidence. For a representative case, the QC-3 waveform, we can impose circular polarization, a frequency and amplitude dependence of the form

$$\omega(t) = \begin{cases} \omega_0 + \alpha_0(t - t_{\omega 0}) & t \leq t_{\omega 0} \\ \omega_0 + \frac{(\omega_0 - \omega_{QNM})(t - t_{\omega 0})}{t_{\omega 0} - t_{\omega 1}} & t_{\omega 0} < t < t_{\omega 1} \\ \omega_{QNM} & t \geq t_{\omega 1} \end{cases} \quad (6.1)$$

$$\sigma(t) = \begin{cases} \sigma_0 & t \leq t_{\sigma 0} \\ \sigma_0 + \frac{(\sigma_0 - \sigma_{QNM})(t - t_{\sigma 0})}{t_{\sigma 0} - t_{\sigma 1}} & t_{\sigma 0} < t < t_{\sigma 1} \\ \sigma_{QNM} & t \geq t_{\sigma 1} \end{cases} \quad (6.2)$$

$$\varphi(t) = \varphi_0 + \int_{t_0}^t \omega(t') dt' \quad (6.3)$$

$$A(t) = e^{a_0 + \int_{t_0}^t \sigma(t') dt'} \quad (6.4)$$

$$r\psi_4 = A(t) e^{-i\varphi(t)}. \quad (6.5)$$

A simple interpretation of the parametrization we have chosen for the plunge waveform starts from the amplitude-phase representation of the waveform  $r\psi_4$  as above. We then model the time dependence of the orbital frequency of the last stage of the inspiral by a linear increase that changes slope through the plunge piece of the waveform and then matched the final quasi-normal frequency of the ringing down remnant black hole. For the time variation of the amplitude we have chosen to match between an initial exponential growth and a final exponential decay.

The quantities labeled “QNM” are set to their expected values for the least damped quasi-normal mode from black hole perturbation theory, in this case  $\omega_{QNM} = 0.55$  and  $\sigma_{QNM} = -0.073$ . The quantity  $\alpha_0$  is chosen informally to have the value 0.0085. The other eight quantities are chosen by non-linear least-squares fit to have the approximate respective values  $\{\omega_0 = 0.2894, t_{\omega 0} = 33.00, t_{\omega 1} = 67.05, \sigma_0 = 0.2192, t_{\sigma 0} = 32.54, t_{\sigma 1} = 62.92, \varphi_0 = -4.40, a_0 = -6.31\}$ . A comparison of the fit to the original curve is shown in Fig. 36. We plan to further investigate the “fitting” representation of the waveforms to optimize the number and robustness of the parameters to be used as well as the choice of the fitting functions. This will also facilitate the matching of the plunge waveforms with a, for instance, Post-Newtonian one for the inspiral phase.

The curve shown for  $r\psi_4(t)$  displays only the time de-

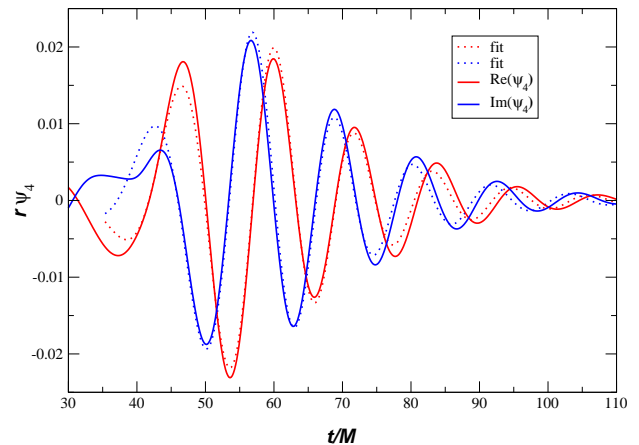


FIG. 36: Comparison with the fitted curve.

pendence. For the full wave information, we have

$$\psi_4(t - r^*, \theta, \varphi) = -_2Y_{22} \psi_4^{(m=+2)}(t - r^*) + -_2Y_{2-2} \psi_4^{(m=-2)}(t - r^*) \quad (6.6)$$

where the  ${}_sY_{lm}$  are spin-weighted spherical harmonics,

$$-_2Y_{22} = \sqrt{5/4\pi} \cos^4(\theta/2) \exp(2i\varphi) \quad (6.7)$$

$$-_2Y_{2-2} = \sqrt{5/4\pi} \sin^4(\theta/2) \exp(-2i\varphi). \quad (6.8)$$

## VII. DISCUSSION

We have produced the first astrophysical model for binary black hole coalescence waveforms. We use the Lazarus method applying the techniques of numerical relativity in the strongly interacting intermediate plunge region and close-limit black hole perturbation theory in the late-time region. As a stand-in for the “far-limit” early part of the dynamics we have taken data from a family of solutions to Einstein’s equations restricted to a space-like slice of spacetime. This Lazarus approach is ideal in this application for which each component treatment is at best marginally applicable by itself. Not only does the Lazarus method expand the scope of treatable problems, but it provides a natural framework for cross-checking the various treatments against each other.

In the first part of the paper we have performed a thorough study of the performance the late-time treatment, including the numerical relativity and close-limit regions on a series of initial data set approaching the fiducial target “ISCO” data, the results of which were recently reported on in Ref. [14]. the present study strongly establishes the effectiveness of our late-time methods.

Our early-time model is based on a selection from one of the standard families of black hole initial data used in numerical relativity, the QC-sequence. Because of the generic uncertainty in describing astrophysically accurate initial data consistent with Einstein’s equations for

strongly interacting black holes, we had little basis, *a priori*, for trusting these data as astrophysically reasonable. Thus, the main part of this paper has addressed the robustness of the overall results against variations in the physical transition point between the early and late-time portions of our model. In other words, we have tested the *kinematically* defined initial data sets against numerical relativistic *dynamics*. The results show an overwhelming correspondence, which strongly suggests that, at least for, non-spinning black holes, the subtleties of selecting initial data are not as consequential to the resulting waveforms as has been generally expected in the community, and supporting our results as a rough first-look at the gravitational radiation which can be expected from the coalescence of equal-mass non-spinning black holes.

We find the radiation to be dominated by circularly polarized,  $l = 2, |m| = 2$  waves radiating 3% of the system's total energy in a few cycles and significant angular momentum, so that the remnant black hole has an angular momentum parameter of roughly  $a \sim 0.7M$ , as we have summarized the results in relation to astrophysical gravitational wave observation observation in the last section.

In the introductory remarks, we noted the importance of having at least a provisional astrophysical coalescence study not only for the results it provides to observers, who need information for developing their observational strategies, but also for the benefit of theorists who wish to direct their effort efficiently toward the purpose of astrophysical application. In this light, we conclude with a characterization, suggested by the results, of the course we will pursue in future work. We first note that past developments in numerical relativity have been critical in our application and have already brought the state of the art to the point where it can be applied astrophysically. One of the great theoretical worries has been that astrophysical initial data for relatively close black holes might require a great deal of further work. Our results suggest this problem may not be critical, but further work is needed when the individual spins of the in-

teracting black holes may become relevant. It will also be interesting to learn how generally this waveform robustness extends when studying other initial data families. A weakness of our present early-time model is that it provides no direct connection to the inspiral radiation, and thus no cross check with post-Newtonian (PN) dynamics. Further work in this direction will benefit from work on initial data which includes PN dynamical radiation information, as well as longer-running numerical simulations allowing us to extend waveforms farther back in time. Considering the waveforms here presented, we are impressed by its simplicity, a simple multipolar description with monotonically increasing frequency and smoothly changing amplitude. However, for systems of strongly spinning black holes or with significantly unequal masses other arguments indicate complicated waveforms resulting from very involved interactions. A significant observationally motivated goal will then be to learn how generally, in the parameter space of plausible black hole pairs, we can expect the qualitatively simple type interaction and radiation. We expect such a characterization to the parameter space to require significant additional effort, but we can begin soon by comparatively studying co-rotational systems and exploring the lowest order spin and unequal mass effects more quickly.

### Acknowledgments

We would like to thank Bernd Brügmann for many discussions. We also wish to thank Bernard Schutz for calling our attention on the importance of the polarization. We are grateful to Miguel Alcubierre and the Cactus Team lead by Ed Seidel for help on numerical issues related to this work. M.C. was partially supported by a Marie-Curie Fellowship (HPMF-CT-1999-00334). Our full numerical computations have been implemented within the performed at AEI, NCSA, and Leibniz Rechenzentrum.

- 
- [1] A. A. Abramovici, W. Althouse, R. P. Drever, Y. Gursel, S. Kawamura, F. Raab, D. Shoemaker, L. Sievers, R. Spero, K. S. Thorne, R. Vogt, R. Weiss, S. Whitcomb, and M. Zucker, *Science* **256**, 325 (1992).
  - [2] C. Bradaschia and et al., *Nucl. Instr. Meth. A.* **289**, 518 (1990).
  - [3] S. P. Zwart and S. McMillan, *ApJ. Lett.* **528**, L17 (2000).
  - [4] S. P. Zwart and S. McMillan, *Int. J. of Mod. Physics A.* **Vol. 15, No. 30**, 4871 (2000).
  - [5] J. Hough, (1994), prepared for Edoardo Amaldi Meeting on Gravitational Wave Experiments, Rome, Italy, 14-17 Jun 1994.
  - [6] E. B. Schutz, *Classical and Quantum Gravity* **18**, 3965 (2001).
  - [7] Éanna É. Flanagan and S. A. Hughes, *Phys. Rev. D* **57**, 4566 (1998).
  - [8] T. Damour, B. R. Iyer, and B. S. Sathyaprakash, *Phys. Rev.* **D63**, 044023 (2001).
  - [9] S. A. Hughes, S. Marka, P. L. Bender, and C. J. Hogan, (2001).
  - [10] For the Binary Black Hole Grand Challenge, see [www.npac.syr.edu/projects/bh/](http://www.npac.syr.edu/projects/bh/).
  - [11] S. Brandt, R. Correll, R. Gomez, M. Huq, P. Laguna, L. Lehner, P. Marronetti, R. A. Matzner, D. Neilsen, J. Pullin, E. Schnetter, D. Shoemaker, and J. Winicour, *Phys. Rev. Lett.* **85**, 5496 (2000).
  - [12] M. Alcubierre, W. Bengert, B. Brügmann, G. Lanfermann, L. Nerger, E. Seidel, and R. Takahashi, *Phys. Rev. Lett.* **87**, 271103 (2001), gr-qc/0012079.
  - [13] J. Baker, S. R. Brandt, M. Campanelli, C. O. Lousto, E. Seidel, and R. Takahashi, *Phys. Rev. D* **62**, 127701

- (2000), gr-qc/9911017.
- [14] J. Baker, B. Brügmann, M. Campanelli, C. O. Lousto, and R. Takahashi, Phys. Rev. Letters **87**, 121103 (2001).
- [15] G. B. Cook, Phys. Rev. D **50**, 5025 (1994).
- [16] T. W. Baumgarte, Phys. Rev. D **62**, 024018 (2000).
- [17] A. Buonanno and T. Damour, Phys. Rev. **D62**, 064015 (2000).
- [18] J. Baker, M. Campanelli, and C. O. Lousto, Phys. Rev. D **65**, 044001 (2001).
- [19] S. A. Teukolsky, Astrophys. J. **185**, 635 (1973).
- [20] C. O. Lousto, Phys. Rev. **D63**, 047504 (2001).
- [21] J. Baker, B. Brügmann, M. Campanelli, and C. O. Lousto, Class. Quantum Grav. **17**, L149 (2000).
- [22] J. Baker, A. Abrahams, P. Anninos, S. Brandt, R. Price, J. Pullin, and E. Seidel, Phys. Rev. D **55**, 829 (1997).
- [23] P. Anninos, R. H. Price, J. Pullin, E. Seidel, and W.-M. Suen, Phys. Rev. D **52**, 4462 (1995).
- [24] J. Bowen and J. W. York, Phys. Rev. D **21**, 2047 (1980).
- [25] S. Brandt and B. Brügmann, Phys. Rev. Lett. **78**, 3606 (1997).
- [26] P. Marronetti and R. Matzner, Phys. Rev. Lett. **85**, 5500 (2000), gr-qc/0009044.
- [27] P. Grandclement, E.ourgoulhon, and S. Bonazzola, Phys. Rev. D **65**, 044021 (2001).
- [28] G. B. Cook, (2001), gr-qc/0108076.
- [29] S. Dain, C. O. Lousto, and R. Takahashi, (2002), gr-qc/0201062.
- [30] B. Brügmann, M. Campanelli, P. Diener, and W. Tichy, in preparation (unpublished).
- [31] <http://www.cactuscode.org>.
- [32] M. Alcubierre, G. Allen, B. Brügmann, E. Seidel, and W.-M. Suen, Phys. Rev. D **62**, 124011 (2000), gr-qc/9908079.
- [33] J. Baker and M. Campanelli, Phys. Rev. D **62**, 127501 (2000).
- [34] M. Alcubierre, S. Brandt, B. Brügmann, C. Gundlach, J. Massó, and P. Walker, Class. Quantum Grav. **17**, 2159 (2000), gr-qc/9809004.
- [35] F. Echeverría, Phys. Rev. D **40**, 3194 (1989).
- [36] R. Gleiser, G. Khanna, R. H. Price, and J. Pullin, New Jour. Phys. **2**, 3 (2000).
- [37] S. Frittelli and R. Gomez, J. Math. Phys. **41**, 5535 (2000).
- [38] M. Campanelli and C. O. Lousto, Phys. Rev. D **59**, 124022 (1999).
- [39] A. Abrahams and R. Price, Phys. Rev. D **53**, 1972 (1996).
- [40] A. Buonanno and T. Damour, Phys. Rev. **D59**, 084006 (1999).
- [41] T. Damour, P. Jaranowski, and G. Schafer, Phys. Rev. **D62**, 084011 (2000).
- [42] T. Damour, P. Jaranowski, and G. Schafer, Phys. Lett. **B513**, 147 (2001).
- [43] T. Damour, B. R. Iyer, and B. S. Sathyaprakash, Phys. Rev. **D57**, 885 (1998).
- [44] L. Blanchet, (2001), gr-qc/0112056.
- [45] T. Damour, P. Jaranowski, and G. Schafer, Phys. Rev. **D63**, 044021 (2001).
- [46] L. Blanchet, B. R. Iyer, C. M. Will, and A. G. Wiseman, Class. Quant. Grav. **13**, 575 (1996).
- [47] Note that in Ref. [14] we have underestimated the angular momentum radiated due to a mistake in the coding of  $\dot{J}$  expression.
-